Effects of electronic relaxation processes on vibrational linewidths of adsorbates on surfaces: The case of CO/Cu(100)

D. Novko,[1] M. Alducin,[1,2] M. Blanco-Rey,[1,3] and J. I. Juaristi[1,2,3]

[1]*Donostia International Physics Center (DIPC), Paseo Manuel de Lardizabal 4, 20018 Donostia-San Sebastián, Spain*

[2]*Centro de Física de Materiales CFM/MPC (CSIC-UPV/EHU), Paseo Manuel de Lardizabal 5, 20018 Donostia-San Sebastián, Spain*

[3]*Departamento de Física de Materiales, Facultad de Químicas UPV/EHU, Apartado 1072, 20080 Donostia-San Sebastián, Spain*

(Received 7 September 2016; published 30 December 2016)

We investigate nonadiabatic effects for the vibrational stretch mode of the CO molecule adsorbed on the top site of the Cu(100) surface. By studying the long-wavelength ($\mathbf{q} \approx 0$) imaginary and real parts of the density functional theory based phonon self-energy due to the electron-phonon coupling Π_λ we obtain the phonon linewidth and the frequency renormalization of the CO stretch mode, respectively. To simulate electronic scattering processes that lead to further damping of the phonon modes we include a phenomenological damping in the phonon self-energy, as well as in the single-electron spectral function that enters Π_λ, through the momentum distribution function. For the specific case of electron-impurity scattering we explicitly show how this process opens the indirect intraband channel and broadens the linewidth of the CO stretch mode. To emphasize the importance of accounting for electronic scattering processes we compare the phonon linewidths in the clean noninteracting limit (infinite electron lifetime) and when electronic scattering processes are phenomenologically included (finite electron lifetime) with available experimental data. We find that the agreement with experiments is improved in the latter case.

DOI: 10.1103/PhysRevB.94.224306

I. INTRODUCTION

The adiabatic Born-Oppenheimer approximation (BOA) is considered to be the foundation for the ground state electronic and ionic calculations, i.e., electronic and phononic band structures [1]. Although this is fundamentally valid only for systems where the energies of the electronic excitations are much larger than the vibrational energies (adiabaticity) [2], as in insulators and semiconductors, the BOA generally gives a very good description of phonon dispersion in metallic systems [3], where the adiabatic condition is not met. From theoretical considerations it was demonstrated that nonadiabatic effects should lead to the renormalization of the optical phonon spectrum, as well as to the appearance of the corresponding phonon linewidth [4–7]. Even though these effects are considered to be hard to observe in bulk systems [8,9], it was recently shown within the framework of Raman spectroscopy that they could be important for explaining the long-wavelength ($\mathbf{q} \approx 0$) part of the phonon spectrum of layered graphene-based systems [10–14].

Very similar and equally interesting is the problem of dynamical effects of adsorbed atomic and molecular species on metallic surfaces. Here, the importance of nonadiabatic corrections was originally demonstrated through the finite vibrational linewidths of the adsorbate high-frequency modes that come from electron-phonon coupling (see Ref. [15] and references therein). Namely, it was shown how the lifetime of vibrationally excited dipolar molecules is substantially reduced from the millisecond regime in the gas phase to the picosecond regime on various metallic surfaces. More recently, evidence of nonadiabaticity was manifested experimentally in the so-called chemicurrents, which are electrical currents generated upon adsorption of atomic and molecular species on metal surfaces [16–18]. Similarly, excited electrons are observed when highly vibrational excited molecules collide with a metal surface [19,20]. The corresponding theoretical work also emerged to explain these effects, either by using isotropic friction coefficients in molecular dynamics simulations [21–30] or by calculating the vibrational damping rate with the Fermi golden rule formula [31–42]. The latter expression has been also used to describe the diffusion of subsurface H towards a Pd(111) surface induced by the scanning tunneling microscope [43].

In the aforementioned cases (bulk systems and adsorbed molecules on surfaces) the key physical quantity for understanding nonadiabatic effects on the vibrational spectra is the phonon self-energy due to electron-phonon coupling, $\Pi_\lambda(\mathbf{q},\omega)$ (here $\mathbf{q}$ and ω are the momentum and frequency of the excitation and λ denotes the phonon mode). The static part of this phonon self-energy, $\Pi_\lambda(\mathbf{q},0)$ ($\omega \ll |\varepsilon_\alpha - \varepsilon_\beta|$, where $\varepsilon_{\alpha,\beta}$ are the eigenvalues of the electronic states α and β involved in the coupling), is relevant for obtaining the adiabatic phonon frequencies [44], while the dynamic part, $\Pi_\lambda(\mathbf{q},\omega \neq 0)$, gives information on nonadiabatic effects. Specifically, its imaginary part is related to the phonon linewidth, while its real part renormalizes the phonon frequency. In usual vibrational spectroscopy experiments (e.g., infrared and Raman spectroscopies) the electromagnetic field is used as the external perturbation. Therefore, the relevant phonon self-energy for describing these experimental results is the long-wavelength part of this self-energy, $\Pi_\lambda(\mathbf{q} \approx 0,\omega)$ [45]. It has been shown that this $\mathbf{q} \approx 0$ part is considerably affected by the relaxation processes of the electronic system (e.g., electron scattering on phonons, impurities, or other electrons) [6,7,46–48], in a close analogy with the $\mathbf{q} \approx 0$ part of the Kubo conductivity formula [49–55] and the electronic Raman correlation function [56–60]. More specifically, the intraband part goes to zero in the clean (impurity free) noninteracting limit, while it takes a finite value when electron relaxation processes are considered. In fact, for high vibrational frequencies, $\omega_{\mathbf{q}\lambda} \gg |\varepsilon_\alpha - \varepsilon_\beta|$, it is proportional to $(\omega\tau_{\text{tr}})^{-1}$ [6,60,61], where τ_{tr} is the electron

transport relaxation time. These scattering processes affect the interband part in a similar manner as well [62].

In this paper we analyze the density functional theory (DFT) based phonon self-energy due to the electron-phonon coupling with emphasis on the mentioned electronic relaxation processes. To account for these relaxation processes we use the relaxation time approximation (RTA), where the frequency and momentum dependent damping function, the so-called electron-hole (*e*-*h*) self-energy [53], is replaced by the variable parameter Γ. This way of treating the phonon self-energy can be useful for those numerical calculations where the broadening parameter, used for summation over the momentum space, has a finite value [34–38,41]. In fact, the present approach to accounting for electronic relaxation processes is more general and can be applied to problems of long-wavelength conductivity [53,54] and electronic Raman scattering [60,61,63]. This is due to the two-particle propagator form of the phonon self-energy, which is the essential part of the general correlation function. Extending this formalism to other physical problems is equivalent to changing the electron-phonon vertex by the corresponding vertex (e.g., Raman vertex in the case of electronic Raman scattering).

As a case study we select the stretch mode of an ordered CO molecular layer adsorbed on the Cu(100) surface, which was one of the first examples that revealed the importance of nonadiabatic corrections for the vibrational lifetimes of adsorbates on metal surfaces. The earliest experiments done on this system with infrared absorption spectroscopy (IRAS) reported vibrational lifetimes in the range $\tau = 1.2$–1.4 ps, or the corresponding linewidths $\gamma = 110$–140 GHz [64,65]. The slight change of the linewidth with surface temperature observed in Ref. [65] ($\delta\gamma \approx 11$ GHz within the range $T = 100$–160 K) was attributed to pure dephasing, where the high-frequency CO stretch mode couples anharmonically to the low-frequency frustrated translational mode. Nevertheless, this effect on the linewidth is relatively small and the excitation of *e*-*h* pairs is still considered to be the relevant damping channel [66]. Later pump-probe laser spectroscopy experiments reported lifetimes on the same order of magnitude, $\tau = 2 \pm 1$ ps ($\gamma = 80 \pm 40$ GHz) [67]. These experimental results were modeled by many theoretical calculations [26,31,32,34,36,37,41,42]. However, none of these studies performed a clear distinction between the $\mathbf{q} \approx 0$ intraband and interband contributions, nor did they consider the case where the phonon relaxation rate due to electron-phonon coupling is additionally triggered by electronic scattering processes [68]. In this paper we do so.

The paper is organized as follows. In Sec. II we present the general theory for obtaining nonadiabatic effects in the electron-phonon system by defining the phonon propagator and the corresponding phonon self-energy. Using this general formulation as the starting point, in Sec. II A we derive the bare phonon self-energy valid in the clean noninteracting regime. In Sec. II B we introduce the electronic damping rate in a phenomenological way (RTA). A discussion on the effects of long-range screening on the bare phonon self-energy is given in Sec. II C. In Sec. II D we derive the high-energy intraband phonon self-energy relevant for large (optical) phonon frequencies and in the presence of impurities

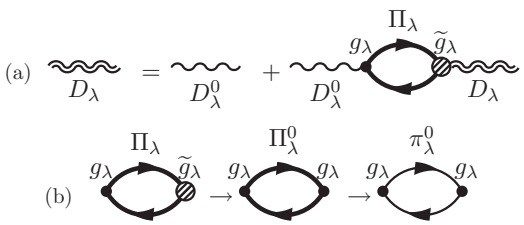

FIG. 1. Diagrammatic representation of (a) the Dyson equation for the phonon propagator D_λ and (b) the reduction of the exact phonon self-energy Π_λ to the bare one π^0_λ. The thick lines correspond to the exact Green's function G, while the thin lines to the bare G^0. The bare and dressed electron-phonon vertex functions are labeled g_λ and $\widetilde{g}_\lambda$, respectively.

(dirty regime). The validity of the quasistatic approximation of the phonon self-energy in evaluating the linewidth of high-frequency vibrational modes is discussed in Sec. II E. The results of our calculations are given in Sec. III, where we give the computational details, geometric and electronic structure, phonon linewidths, and renormalized phonon frequencies for the CO stretch mode on Cu(100) in Secs. III A, III B, III C, and III D, respectively. Finally, we present the concluding remarks in Sec. IV. In this paper atomic units ($m_e = e = \hbar = 1$) are used unless otherwise stated.

II. THEORY

The frequency representation of the free phonon propagator of mode λ is given in Matsubara notation by the well known result [55,69]

$$D^0_\lambda(\mathbf{q}, i\nu_n) = \frac{2\omega_{\mathbf{q}\lambda}}{(i\nu_n)^2 - \omega^2_{\mathbf{q}\lambda}}, \tag{1}$$

where $i\nu_n$ are the Matsubara frequencies for bosons, and $\omega_{\mathbf{q}\lambda}$ is the bare frequency of the phonon mode λ. By doing the analytical continuation ($i\nu_n \rightarrow \omega + i\eta$) of Eq. (1) we get the function $D^0_\lambda(\mathbf{q},\omega)$, where the imaginary part gives us the spectrum of the bare phonons (density of the bare phonon states).

To get a more realistic description of the phonon spectrum, we need to introduce the electron-phonon coupling in our system and solve the Dyson equation represented diagrammatically in Fig. 1(a). According to this equation the renormalized phonon propagator can be written as

$$D_\lambda(\mathbf{q}, i\nu_n) = \frac{2\omega_{\mathbf{q}\lambda}}{(i\nu_n)^2 - \omega^2_{\mathbf{q}\lambda} - 2\omega_{\mathbf{q}\lambda}\Pi_\lambda(\mathbf{q}, i\nu_n)}, \tag{2}$$

where $\Pi_\lambda(\mathbf{q},\omega)$ is the phonon self-energy due to electron-phonon coupling. In systems where the harmonic approximation does not hold, phonon-phonon coupling effects (anharmonicity) should also be taken into account, i.e., $\Pi_\lambda = \Pi^{\text{el-ph}}_\lambda + \Pi^{\text{ph-ph}}_\lambda$. However, in our present study we restrict ourselves to the electron-phonon coupling only. The exact phonon self-energy due to electron-phonon coupling is represented by the first bubble diagram in Fig. 1(b) [4,44,70]

and we can write it as

$$\Pi_\lambda(\mathbf{q},i\nu_n) = \sum_{\mu\mu'\mathbf{k}\sigma} \frac{1}{\beta}\sum_{i\omega_n} \left[g_\lambda^{\mu\mu'}(\mathbf{k},\mathbf{q})\right]^* \tilde{g}_\lambda^{\mu\mu'}(\mathbf{k},\mathbf{q},i\omega_n,i\nu_n) \times G_\mu(\mathbf{k},i\omega_n)G_{\mu'}(\mathbf{k}+\mathbf{q},i\omega_n+i\nu_n), \quad (3)$$

where μ,μ' are the electronic band indices, the summation over σ accounts for the spin degrees of freedom, and the inverse of the temperature is $\beta = 1/(k_B T)$. One of the vertex functions is the bare electron-phonon vertex in the harmonic approximation

$$g_\lambda^{\mu\mu'}(\mathbf{k},\mathbf{q}) = \frac{1}{\sqrt{2M_\lambda\omega_{\mathbf{q}\lambda}}}\langle\psi_{\mu'\mathbf{k}+\mathbf{q}}|\frac{\partial V_{ei}}{\partial \mathbf{Q}_{\mathbf{q}\lambda}}\cdot\boldsymbol{\epsilon}_{\mathbf{q}\lambda}|\psi_{\mu\mathbf{k}}\rangle \equiv \frac{1}{\sqrt{2M_\lambda\omega_{\mathbf{q}\lambda}}} d_\lambda^{\mu\mu'}(\mathbf{k},\mathbf{q}), \quad (4)$$

while the other, $\tilde{g}_\lambda^{\mu\mu'}(\mathbf{k},\mathbf{q},i\omega_n,i\nu_n)$, is dressed (renormalized) with higher-order scattering processes, i.e., with vertex corrections and single-particle self-energy contributions that come from electron-electron, electron-phonon, or electron-impurity scatterings. The wave functions $\psi_{\mu\mathbf{k}}$ are the ground state one-electron wave functions, $\varepsilon_{\mu\mathbf{k}}$ are the corresponding eigenvalues, and V_{ei} is the electron-ion potential energy. For each phonon with wave vector $\mathbf{q}$ and branch λ there is an associated effective mass M_λ, a bare phonon frequency $\omega_{\mathbf{q}\lambda}$, and a displacement $\mathbf{Q}_{\mathbf{q}\lambda} = Q_{\mathbf{q}\lambda}\boldsymbol{\epsilon}_{\mathbf{q}\lambda}$, where $\boldsymbol{\epsilon}_{\mathbf{q}\lambda}$ is a unit length polarization vector. Each of the Matsubara Green's functions in Eq. (3) satisfy the corresponding Dyson equation

$$G_\mu(\mathbf{k},i\omega_n) = \frac{1}{i\omega_n - \varepsilon_{\mu\mathbf{k}} - \Sigma_\mu(\mathbf{k},i\omega_n)}, \quad (5)$$

where $\Sigma_\mu(\mathbf{k},i\omega_n)$ is the single-electron self-energy. This Dyson equation can be used to express Eq. (3) in a slightly different form

$$\Pi_\lambda(\mathbf{q},i\nu_n) = \sum_{\mu\mu'\mathbf{k}\sigma} \frac{1}{\beta}\sum_{i\omega_n} \left[g_\lambda^{\mu\mu'}(\mathbf{k},\mathbf{q})\right]^* \tilde{g}_\lambda^{\mu\mu'}(\mathbf{k},\mathbf{q},i\omega_n,i\nu_n) \times \frac{G_\mu(\mathbf{k},i\omega_n) - G_{\mu'}(\mathbf{k}+\mathbf{q},i\omega_n+i\nu_n)}{i\nu_n + \varepsilon_{\mu\mathbf{k}} - \varepsilon_{\mu'\mathbf{k}+\mathbf{q}} + \Delta\Sigma_{\mu\mu'}(\mathbf{k},\mathbf{q},i\omega_n,i\nu_n)}, \quad (6)$$

where we define the bare *e-h* self-energy $\Delta\Sigma_{\mu\mu'}(\mathbf{k},\mathbf{q},i\omega_n,i\nu_n) \equiv \Sigma_\mu(\mathbf{k},i\omega_n) - \Sigma_{\mu'}(\mathbf{k}+\mathbf{q},i\omega_n+i\nu_n)$ [53]. From this form of the phonon self-energy we can see what the role of the *e-h* self-energy is as follows: its real part renormalizes the electronic structure (i.e., $\varepsilon_{\mu\mathbf{k}}$), while its imaginary part gives additional damping to the phonon spectrum.

The analytical continuation of expression (2) is of great interest because its imaginary part gives the spectral function of the phonon excitations that corresponds to the experimental spectra (e.g., IRAS). The phonon linewidth (relaxation rate due to *e-h* pair excitations) and the renormalized phonon frequency are then respectively given by

$$\gamma_{\mathbf{q}\lambda} = -2\mathrm{Im}\Pi_\lambda(\mathbf{q},\omega_{\mathbf{q}\lambda}) \quad (7)$$

and

$$\omega^2 = \omega_{\mathbf{q}\lambda}^2 + 2\omega_{\mathbf{q}\lambda}\mathrm{Re}\Pi_\lambda(\mathbf{q},\omega), \quad (8)$$

where Eq. (8) needs to be calculated self-consistently. If one is interested in electronic excitations (e.g., single-electron excitations or plasmons), it is useful to know that the spectral function of the phonon excitations shares close resemblance with the energy loss function, $\mathrm{Im}\,\varepsilon^{-1}(\mathbf{q},\omega)$, but then $\omega_{\mathbf{q}\lambda}$ and Π_λ would have to be replaced by the bare plasmon energy and the appropriate current-current correlation function, respectively [54,71,72]. In that case Eq. (7) would give the plasmon linewidth, while Eq. (8) the renormalization of its energy.

A. Bare phonon self-energy

The first step of our analysis consists of obtaining the bare phonon self-energy and examining its general properties. We define the bare phonon self-energy as in the third bubble diagram of Fig. 1(b), i.e., without vertex corrections and with the exact Green's function [Eq. (5)] replaced by the bare one,

$$G_\mu^0(\mathbf{k},i\omega_n) = \frac{1}{i\omega_n - \varepsilon_{\mu\mathbf{k}}}. \quad (9)$$

By doing this the phonon self-energy is reduced to a form that describes the ideal electron-phonon system, where impurities and the electron-electron interaction are disregarded, as well as higher orders of the electron-phonon interaction. For systems in which these scattering processes do not play an important role, the bare phonon self-energy serves as a good approximation for obtaining the phonon spectra. After considering the above mentioned steps and doing the analytical continuation, we get the following form for the bare phonon self-energy [5,48]:

$$\pi_\lambda^0(\mathbf{q},\omega) = \sum_{\mu\mu'\mathbf{k}\sigma} \left|g_\lambda^{\mu\mu'}(\mathbf{k},\mathbf{q})\right|^2 \frac{f_{\mu\mathbf{k}} - f_{\mu'\mathbf{k}+\mathbf{q}}}{\omega + \varepsilon_{\mu\mathbf{k}} - \varepsilon_{\mu'\mathbf{k}+\mathbf{q}} + i\eta}, \quad (10)$$

where $\eta \to 0^+$ and $f_{\mu\mathbf{k}} = (1/\beta)\sum_{i\omega_n} G_\mu^0(\mathbf{k},i\omega_n)$ is the temperature-dependent Fermi-Dirac distribution function.

To get a closer insight into the bare phonon self-energy and to understand what kind of electronic excitations are involved in it, we decompose it into its intraband ($\mu = \mu'$) and interband ($\mu \neq \mu'$) contributions, i.e.,

$$\pi_\lambda^0(\mathbf{q},\omega) = \pi_\lambda^{\mathrm{intra},0}(\mathbf{q},\omega) + \pi_\lambda^{\mathrm{inter},0}(\mathbf{q},\omega). \quad (11)$$

Due to the long-wavelength nature of the electromagnetic field in infrared spectroscopy experiments, our main concern is the $\mathbf{q} \approx 0$ phonons. In that case we can expand the intraband part of expression (10) into powers of small $\mathbf{q}$ and write the first nonzero term as

$$\pi_\lambda^{\mathrm{intra},0}(\omega) = \sum_{\mu\mathbf{k}\sigma,\alpha\beta} \frac{\left|g_\lambda^{\mu\mu}(\mathbf{k},0)\right|^2}{(\omega+i\eta)^2} f_{\mu\mathbf{k}} \frac{\partial^2\varepsilon_{\mu\mathbf{k}}}{\partial k_\alpha \partial k_\beta} q_\alpha q_\beta, \quad (12)$$

where we write $\pi_\lambda^{\mathrm{intra},0}(\mathbf{q}\approx 0,\omega) \equiv \pi_\lambda^{\mathrm{intra},0}(\omega)$ to simplify the notation. This expression allows us to extract already some important conclusions about the nature of the bare $\mathbf{q}\approx 0$ intraband phonon self-energy: (i) the terms of order q^0 and q^1 are zero, so when $q \to 0$ then $\pi_\lambda^{\mathrm{intra},0} \to 0$ as q^2; (ii) the dependence q^2/ω^2 resembles the Lindhard-like form of the charge-charge correlation function if $|g_\lambda^{\mu\mu}(\mathbf{k},0)|$ is replaced with the bare charge vertex $|\rho^{\mu\mu}(\mathbf{k},0)| \approx 1$ [73]; (iii) the imaginary part is proportional to $\delta(\omega)/\omega$, where $\delta(\omega)$ is the

Dirac delta function, and thus only the acoustic phonons are damped.

The interband part for $\mathbf{q} \approx 0$ is

$$\pi_{\lambda}^{\text{inter},0}(\omega) = \sum_{\mu\neq\mu',\mathbf{k}\sigma} \left|g_{\lambda}^{\mu\mu'}(\mathbf{k},0)\right|^2 \frac{f_{\mu\mathbf{k}} - f_{\mu'\mathbf{k}}}{\omega + \varepsilon_{\mu\mathbf{k}} - \varepsilon_{\mu'\mathbf{k}} + i\eta}. \quad (13)$$

Here $f_{\mu\mathbf{k}} \neq f_{\mu'\mathbf{k}}$, which in principle makes the $\mathbf{q} \approx 0$ interband self-energy finite for all phonon (acoustic and optical) modes. We write the imaginary and real parts of the latter contribution as

$$\text{Im}\pi_{\lambda}^{\text{inter},0}(\omega) = -\pi \sum_{\mu\neq\mu',\mathbf{k}\sigma} \left|g_{\lambda}^{\mu\mu'}(\mathbf{k},0)\right|^2 (f_{\mu\mathbf{k}} - f_{\mu'\mathbf{k}}) \times \delta(\omega + \varepsilon_{\mu\mathbf{k}} - \varepsilon_{\mu'\mathbf{k}}) \quad (14)$$

and

$$\text{Re}\pi_{\lambda}^{\text{inter},0}(\omega) = \sum_{\mu\neq\mu',\mathbf{k}\sigma} \left|g_{\lambda}^{\mu\mu'}(\mathbf{k},0)\right|^2 \mathcal{P}\frac{f_{\mu\mathbf{k}} - f_{\mu'\mathbf{k}}}{\omega + \varepsilon_{\mu\mathbf{k}} - \varepsilon_{\mu'\mathbf{k}}}, \quad (15)$$

respectively, where $\mathcal{P}$ stands for the principal value. Expressions (7) and (14) show that the linewidth of the $\mathbf{q} \approx 0$ phonon mode is finite due to interband transitions only if the condition $\omega_{\mathbf{q}\lambda} = \varepsilon_{\mu'\mathbf{k}} - \varepsilon_{\mu\mathbf{k}}$ is strictly met. Since we are mainly interested in optical phonon modes, we can safely use the interband part as the total $\mathbf{q} \approx 0$ bare phonon self-energy,

$$\pi_{\lambda}^{0}(\omega) \approx \pi_{\lambda}^{\text{inter},0}(\omega). \quad (16)$$

This result is analogous to the first-order Fermi golden rule formula for the phonon damping rate due to the electron-phonon interaction [74].

The bare phonon frequency $\omega_{\mathbf{q}\lambda}$ that enters the phonon propagator of Eq. (2) is usually calculated within the adiabatic approximation (see Appendix A); thus to avoid the divergent phonon renormalization by counting the adiabatic contribution twice, the bare phonon self-energy of Eq. (10) should be subtracted with its value at $\omega = 0$ (adiabatic part) [5,70,75–79]:

$$\widehat{\pi}_{\lambda}^{0}(\mathbf{q},\omega) = \pi_{\lambda}^{0}(\mathbf{q},\omega) - \pi_{\lambda}^{0}(\mathbf{q},0) = \sum_{\mu\mu'\mathbf{k}\sigma} \frac{-\omega\left|g_{\lambda}^{\mu\mu'}(\mathbf{k},\mathbf{q})\right|^2}{\varepsilon_{\mu\mathbf{k}} - \varepsilon_{\mu'\mathbf{k}+\mathbf{q}}} \frac{f_{\mu\mathbf{k}} - f_{\mu'\mathbf{k}+\mathbf{q}}}{\omega + \varepsilon_{\mu\mathbf{k}} - \varepsilon_{\mu'\mathbf{k}+\mathbf{q}} + i\eta}. \quad (17)$$

It can be seen from Eq. (17) that this correction can also be done informally by replacing one of the vertex functions $g_{\lambda}^{\mu\mu'}(\mathbf{k},\mathbf{q})$ with $-\omega g_{\lambda}^{\mu\mu'}(\mathbf{k},\mathbf{q})/(\varepsilon_{\mu\mathbf{k}} - \varepsilon_{\mu'\mathbf{k}+\mathbf{q}})$ in Eq. (10) [75]. Since the parameter η is infinitesimal in the bare phonon self-energy, this subtraction only affects the real part of the phonon self-energy (renormalization of the phonon frequency), while the imaginary part stays the same. We will see in Sec. II B that this is not the case in the RTA regime, due to spurious effects that appear when including damping mechanisms in the system by hand.

For the intraband part of the $\mathbf{q} \approx 0$ bare phonon self-energy $\widehat{\pi}_{\lambda}^{0}(\mathbf{q},\omega)$ already the q^0 order term is not zero. Thus, to renormalize the phonon spectrum with $\widehat{\pi}_{\lambda}^{0}(\mathbf{q},\omega)$ both the intraband and interband parts should be included,

$$\text{Re}\widehat{\pi}_{\lambda}^{0}(\omega) = \text{Re}\widehat{\pi}_{\lambda}^{\text{intra},0}(\omega) + \text{Re}\widehat{\pi}_{\lambda}^{\text{inter},0}(\omega). \quad (18)$$

The first term can be expressed as [10,80]

$$\text{Re}\widehat{\pi}_{\lambda}^{\text{intra},0}(\omega) = \lim_{\eta\to 0^+}\left(\frac{\omega^2}{\omega^2+\eta^2}\right) \times \sum_{\mu\mathbf{k}} \left|g_{\lambda}^{\mu\mu}(\mathbf{k},0)\right|^2 \left(-\frac{\partial f_{\mu\mathbf{k}}}{\partial\varepsilon_{\mu\mathbf{k}}}\right) \quad (19)$$

with

$$-\frac{\partial f_{\mu\mathbf{k}}}{\partial\varepsilon_{\mu\mathbf{k}}} = \frac{1}{2k_BT}\frac{1}{1+\cosh\left(\frac{\varepsilon_{\mu\mathbf{k}}-\varepsilon_F}{k_BT}\right)}, \quad (20)$$

where ε_F is the Fermi energy, while the second term is

$$\text{Re}\widehat{\pi}_{\lambda}^{\text{inter},0}(\omega) = \sum_{\mu\neq\mu',\mathbf{k}\sigma} \frac{-\omega\left|g_{\lambda}^{\mu\mu'}(\mathbf{k},0)\right|^2}{\varepsilon_{\mu\mathbf{k}} - \varepsilon_{\mu'\mathbf{k}}} \times \mathcal{P}\frac{f_{\mu\mathbf{k}} - f_{\mu'\mathbf{k}}}{\omega + \varepsilon_{\mu\mathbf{k}} - \varepsilon_{\mu'\mathbf{k}}}. \quad (21)$$

In Eq. (19) we deliberately leave the infinitesimal parameter η to show what the actual dependence on ω is. In the case of optical phonons, this limit is 1. When doing the static limit ($\omega \to 0$) of this expression, the ordering of limits should be reversed, i.e., take first $\omega \to 0$, and then $\eta \to 0$, in order to satisfy the condition $\widehat{\pi}_{\lambda}^{0}(0) = 0$.

B. RTA phonon self-energy

The simplest case of the RTA for the phonon self-energy, in which η is replaced by a phenomenological damping energy $\Gamma > 0$, corresponds to the approximation of Eq. (6) in which (i) the vertex renormalization is neglected, (ii) the exact Matsubara Green's functions in the numerator are replaced with the bare ones, and (iii) only the imaginary part of the bare *e-h* self-energy is kept, but without energy and momentum dependence, i.e., $\Delta\Sigma_{\mu\mu'}(\mathbf{k},\mathbf{q},i\omega_n,i\nu_n) \approx i\text{Im}\Delta\Sigma_{\mu\mu'} \equiv i\Gamma_{\mu\mu'}$. Without this specific structure of the *e-h* self-energy, information on which electrons and phonon modes are responsible for the damping and the breakdown of the momentum conservation law is lost [51,53,55]. Nevertheless, as we are interested in the phonon linewidth for the specific $(\mathbf{q},\lambda)$ mode and not in its functional dependence of ω, in Sec. III C we use a physically meaningful range of $\Gamma_{\mu\mu'}$ and discuss the corresponding linewidths. Following previous works [54,60], it is convenient to distinguish different damping energies for intraband, $\text{Im}\Delta\Sigma_{\mu=\mu'} \equiv \Gamma_{\text{intra}}$, and interband, $\text{Im}\Delta\Sigma_{\mu\neq\mu'} \equiv \Gamma_{\text{inter}}$, transitions. With these approximations we are accounting phenomenologically for electron scattering processes (i.e., electron-electron, electron-phonon, and electron-impurity scattering) that lead to further damping of the phonon spectra. However, the effects of these processes on the renormalization of the electronic band structure are neglected, i.e., $\text{Re}\Delta\Sigma_{\mu\mu'} = 0$. This is a reasonable approximation for weak scattering processes [60,61].

Under these assumptions the $\mathbf{q} \approx 0$ phonon self-energy from Eq. (16) becomes

$$\pi_{\lambda}^{0}(\omega) = \sum_{\mu\neq\mu',\mathbf{k}\sigma} \left|g_{\lambda}^{\mu\mu'}(\mathbf{k},0)\right|^2 \frac{f_{\mu\mathbf{k}} - f_{\mu'\mathbf{k}}}{\omega + \varepsilon_{\mu\mathbf{k}} - \varepsilon_{\mu'\mathbf{k}} + i\Gamma_{\text{inter}}}. \quad (22)$$

This expression shows how the strict condition imposed by the Dirac delta function in $\mathrm{Im}\pi^0_\lambda(\omega)$ for interband transitions [Eq. (14)] is now loosened, and it reads $|\omega+\varepsilon_{\mu\mathbf{k}}-\varepsilon_{\mu'\mathbf{k}}| \lesssim \Gamma_{\mathrm{inter}}/2$.

Similarly, if we apply the same RTA to the phonon self-energy of Eq. (17) (replacing η by $\Gamma_{\mu\mu'}$), we get for $\mathbf{q}\approx 0$

$$\widetilde{\pi}^0_\lambda(\omega)=\sum_{\mu\mu'\mathbf{k}\sigma}\frac{-\omega\left|g^{\mu\mu'}_\lambda(\mathbf{k},0)\right|^2}{\varepsilon_{\mu\mathbf{k}}-\varepsilon_{\mu'\mathbf{k}}}\frac{f_{\mu\mathbf{k}}-f_{\mu'\mathbf{k}}}{\omega+\varepsilon_{\mu\mathbf{k}}-\varepsilon_{\mu'\mathbf{k}}+i\Gamma_{\mu\mu'}}. \tag{23}$$

Comparing Eqs. (22) and (23), it is clear that the imaginary parts of the phonon self-energies π^0_λ and $\widetilde{\pi}^0_\lambda$ within the RTA differ considerably, because now the factor $\omega/(\varepsilon_{\mu\mathbf{k}}-\varepsilon_{\mu'\mathbf{k}})$ of Eq. (23) does not cancel since $\omega\neq\varepsilon_{\mu'\mathbf{k}}-\varepsilon_{\mu\mathbf{k}}$ when $\Gamma_{\mu\mu'}>0$ (see also Appendix D for differences). This implies that the interband parts of these two self-energies are different and, furthermore, that the imaginary part of the phonon self-energy $\widetilde{\pi}^0_\lambda$ has both interband and intraband parts, while the imaginary part of π^0_λ has only the interband contribution for $\mathbf{q}\approx 0$. At this point, it is important to remark that the different behavior of $\widetilde{\pi}^0_\lambda$ with respect to π^0_λ in the RTA is due to the *ad hoc* inclusion of the relaxation processes in Eq. (17), which in fact turns out to be nonphysical. More precisely, in the case of π^0_λ the higher-order diagrammatic expansion of the scattering processes leads naturally to the appearance of a damping energy [7,62], i.e., an *e-h* self-energy, while to our knowledge in the case of $\widetilde{\pi}^0_\lambda$ there is no corresponding perturbation expansion of the Hamiltonian associated with this bare phonon self-energy in the literature (see Appendix A and Ref. [2]). Thus, it is not completely clear how the RTA form of $\widetilde{\pi}^0_\lambda$ should look (see Appendix B for a possible expression of $\widetilde{\pi}^0_\lambda$ in RTA).

Next, we consider the damping effects in π^0_λ a step further than in Eq. (22) and instead of neglecting the dressed single-electron self-energies in the Green's functions appearing in the numerator of Eq. (6), we also account for them phenomenologically. Such a phonon self-energy corresponds to the second bubble diagram in Fig. 1(b), where $\Delta\Sigma_{\mu\mu'}(\mathbf{k},\mathbf{q},i\omega_n,i\nu_n)\to i\Gamma_{\mu\mu'}$, and reads

$$\Pi^0_\lambda(\omega)=\sum_{\mu\neq\mu',\mathbf{k}\sigma}\left|g^{\mu\mu'}_\lambda(\mathbf{k},0)\right|^2\frac{n_\mu(\mathbf{k})-n_{\mu'}(\mathbf{k})}{\omega+\varepsilon_{\mu\mathbf{k}}-\varepsilon_{\mu'\mathbf{k}}+i\Gamma_{\mathrm{inter}}}. \tag{24}$$

In this expression the momentum distribution functions $n_\mu(\mathbf{k})$ appear instead of the usual Fermi-Dirac distribution functions. Approximating $n_\mu(\mathbf{k})$ by $f_{\mu\mathbf{k}}$, as done in Eq. (22), is equivalent to substituting the interacting electron distribution by the thermal equilibrium value for noninteracting electrons. The exact definition of the momentum distribution function is

$$\begin{aligned} n_\mu(\mathbf{k}) &= \frac{1}{\beta}\sum_{i\omega_n}G_\mu(\mathbf{k},i\omega_n)\\ &= \int_{-\infty}^{\infty}\frac{d\varepsilon}{2\pi}A_\mu(\mathbf{k},\varepsilon)f(\varepsilon), \end{aligned} \tag{25}$$

where $f(\varepsilon)$ is the Fermi-Dirac distribution function and $A_\mu(\mathbf{k},\varepsilon)$ is the exact single-electron spectral function

$$A_\mu(\mathbf{k},\varepsilon)=\frac{-2\mathrm{Im}\Sigma_\mu(\mathbf{k},\varepsilon)}{[\varepsilon-\varepsilon_{\mu\mathbf{k}}-\mathrm{Re}\Sigma_\mu(\mathbf{k},\varepsilon)]^2+[\mathrm{Im}\Sigma_\mu(\mathbf{k},\varepsilon)]^2}. \tag{26}$$

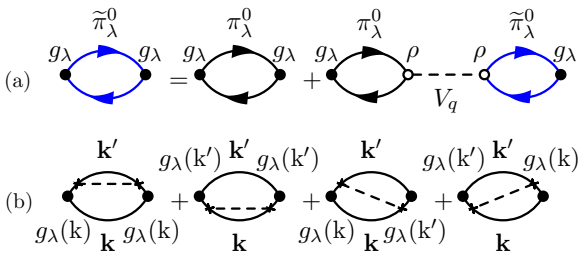

FIG. 2. Diagrammatic representation of (a) the long-range screening of the phonon self-energy π^0_λ and (b) the leading terms in the high-energy expansion of the indirect contribution to the intraband phonon self-energy. The electron-phonon vertex function is represented by g_λ, the charge vertex function by ρ, the bare Coulomb interaction by V_q, and the impurities by crosses.

In our phenomenological approximation, we neglect the real part of the single-electron self-energy, $\mathrm{Re}\Sigma_\mu(\mathbf{k},\varepsilon)=0$, and use a constant damping parameter Γ_μ instead of $-2\mathrm{Im}\Sigma_\mu(\mathbf{k},\varepsilon)$. One further simplification is to use the same damping parameter for all electronic bands μ, i.e., $\Gamma_\mu\equiv\Gamma^A$. This approximation is reasonable in a phenomenological treatment of the intraband relaxation processes of electrons on impurities where the damping of the single-electron spectral function is $-\mathrm{Im}\Sigma_\mu(\mathbf{k},\varepsilon)\approx 1/2\tau_{\mathrm{tr}}$, while the damping of the two-particle propagator (e.g., phonon self-energy or Kubo conductivity formula) is $\mathrm{Im}\Delta\Sigma_{\mu\mu'}(\mathbf{k},\mathbf{q},\omega)\approx 1/\tau_{\mathrm{tr}}$. However, for the interband channel this is no longer the case and this simplification serves just as a coarse estimation. Although the mentioned approximations make the integration in Eq. (25) simpler, it is still a difficult task to perform it analytically for a finite temperature T. As we are only interested in effects of the damping parameter entering $n_\mu(\mathbf{k})$ on the phonon self-energy $\Pi^0_\lambda(\omega)$, we explicitly integrate expression (25) for $T\to 0$ K,

$$n_\mu(\mathbf{k})\approx\frac{1}{2}-\frac{1}{\pi}\tan^{-1}\left[\frac{2(\varepsilon_{\mu\mathbf{k}}-\varepsilon_F)}{\Gamma^A}\right]. \tag{27}$$

We see from the above expression that when the temperature is very low, but we are still considering realistic relaxation processes (e.g., scattering on impurities), the electronic state distribution is still broadened and governed by the intensity of such processes [81].

C. Long-range screening of the phonon self-energy

In this section we analyze how the long-range Coulomb interaction affects the bare phonon self-energy and, in particular, whether it can eliminate the q^2 dependence in the intraband part. When phonon excitations produce charge fluctuations in the electronic gas, the long-range screening should, in principle, influence the phonon linewidth and the frequency renormalization. Inclusion of the long-range screening into the bare phonon self-energy π^0_λ can be done as in Fig. 2(a) [5,60],

$$\widetilde{\pi}^0_\lambda(\mathbf{q},\omega)=\pi^0_\lambda(\mathbf{q},\omega)+\pi^0_{\lambda 0}(\mathbf{q},\omega)V_q\frac{\pi^0_{0\lambda}(\mathbf{q},\omega)}{\epsilon(\mathbf{q},\omega)}, \tag{28}$$

where we have defined a more general form of the correlation function as

$$\pi^0_{\alpha\beta}(\mathbf{q},\omega) = \sum_{\mu\mu'\mathbf{k}\sigma} \left[F^{\mu\mu'}_{\alpha}(\mathbf{k},\mathbf{q})\right]^* F^{\mu\mu'}_{\beta}(\mathbf{k},\mathbf{q}) \times \frac{f_{\mu\mathbf{k}} - f_{\mu'\mathbf{k}+\mathbf{q}}}{\omega + \varepsilon_{\mu\mathbf{k}} - \varepsilon_{\mu'\mathbf{k}+\mathbf{q}} + i\eta}, \tag{29}$$

$$F^{\mu\mu'}_{\alpha}(\mathbf{k},\mathbf{q}) = \begin{cases} g^{\mu\mu'}_{\lambda}(\mathbf{k},\mathbf{q}), & \text{for } \alpha = \lambda, \\ \rho^{\mu\mu'}(\mathbf{k},\mathbf{q}), & \text{for } \alpha = 0. \end{cases} \tag{30}$$

Here we have introduced the charge vertex function $\rho^{\mu\mu'}(\mathbf{k},\mathbf{q}) = \langle\psi_{\mu\mathbf{k}}|e^{-i\mathbf{q}\cdot\mathbf{r}}|\psi_{\mu'\mathbf{k}+\mathbf{q}}\rangle$, the bare Coulomb interaction V_q, and the dielectric screening function

$$\epsilon(\mathbf{q},\omega) = 1 - V_q\chi(\mathbf{q},\omega). \tag{31}$$

The function $\chi(\mathbf{q},\omega)$ is the charge-charge correlation function given by $\pi^0_{00}(\mathbf{q},\omega)$ and the function $\pi^0_{\lambda 0}(\mathbf{q},\omega)$ represents the electron-mediated coupling of the phonon mode λ to the external scalar field. We can look now separately into the screening of the long-wavelength intraband and interband phonon self-energies.

In the long-wavelength limit $\mathbf{q} \approx 0$, Eq. (28) has the form

$$\widetilde{\pi}^0_{\lambda}(\omega) = \pi^0_{\lambda}(\omega) - \frac{\pi^0_{\lambda 0}(\omega)\pi^0_{0\lambda}(\omega)}{\chi(\omega)}, \tag{32}$$

where the essential difference between the intraband and interband contributions is in the corresponding vertex functions,

$$\rho^{\mu\mu'}(\mathbf{k},\mathbf{q}\approx 0) = \begin{cases} 1, & \text{for } \mu = \mu', \\ \frac{-\mathbf{q}\cdot\mathbf{J}^{\mu\mu'}(\mathbf{k},\mathbf{q}\approx 0)}{\varepsilon_{\mu\mathbf{k}} - \varepsilon_{\mu'\mathbf{k}}}, & \text{for } \mu \neq \mu'. \end{cases} \tag{33}$$

The relation between the charge $\rho^{\mu\mu'}(\mathbf{k},\mathbf{q}\approx 0)$ and the current $\mathbf{J}^{\mu\mu'}(\mathbf{k},\mathbf{q}\approx 0)$ vertex functions is derived using the charge continuity equation for the operators [73]. Now, the symmetry of the vertex function product in $\pi^0_{\lambda 0}(\omega)$ governs the degree of phonon self-energy screening; i.e., when the product $[g^{\mu\mu'}_{\lambda}(\mathbf{k},0)]^*\rho^{\mu\mu'}(\mathbf{k},0)$ is an odd function of $\mathbf{k}$ the function $\pi^0_{\lambda 0}(\omega)$ vanishes and when it is even it does not. For example, the vibrational modes of CO adsorbed vertically on the $c(2\times 2)$ unit cell of Cu(100) belong to the C_{4v} point group symmetry, where the CO stretch mode corresponds to the A_1 irreducible representation. In that case $g^{\mu\mu'}_{\lambda=A_1}(\mathbf{k},0)$ is an even function, so $\pi^{\text{intra},0}_{A_1 0}(\omega)$ will be finite, while $\pi^{\text{inter},0}_{A_1 0}(\omega)$ will vanish due to the odd character of $\mathbf{J}^{\mu\mu'}(\mathbf{k},0)$. Thus, when Eqs. (32) and (33) are combined, it can be easily seen that the long-range screening does not affect the interband channel, while the intraband contribution is modified, i.e.,

$$\widetilde{\pi}^{\text{inter},0}_{\lambda}(\omega) \approx \pi^{\text{inter},0}_{\lambda}(\omega) \tag{34}$$

and

$$\widetilde{\pi}^{\text{intra},0}_{\lambda}(\omega) \approx \pi^{\text{intra},0}_{\lambda}(\omega) - \frac{\pi^{\text{intra},0}_{\lambda 0}(\omega)\pi^{\text{intra},0}_{0\lambda}(\omega)}{\chi^{\text{intra}}(\omega)}. \tag{35}$$

Since the long-wavelength intraband part of the correlation function $\pi^0_{\alpha\beta}(\mathbf{q},\omega)$ has the same dependence on q as Eq. (12), we can observe from the last expression that the screened intraband part is still proportional to q^2 [5], and thus is still negligible for the $\mathbf{q} \approx 0$ case.

In contemporary *ab initio* calculations screening effects of the phonon self-energy are implemented in a different but closely related way. In principle, the inner bubble diagrams connected with Coulomb interactions should be all gathered within one of the electron-phonon vertex functions, while the remaining vertex should be bare (e.g., as in Ref. [74]). This new screened electron-phonon vertex function is then frequency dependent. However, in DFT calculations both vertex functions are screened and are usually treated within the adiabatic (static) approximation for practical reasons [70].

D. High-energy expansion of the intraband phonon self-energy

In the preceding analysis of the intraband part of the phonon self-energy we were only considering direct transitions, i.e., those where an electron with momentum $\mathbf{k}$ is directly scattered to the state $\mathbf{k}+\mathbf{q}$ by absorbing the energy of a phonon with momentum $\mathbf{q}$ [first term in Eq. (C7)]. As we already saw in Sec. II A, this process is proportional to q^2, and thus negligible for the $\mathbf{q} \approx 0$ phonons. However, this result does not completely exclude the existence of intraband transitions contributing to the phonon self-energy. In addition to the mentioned direct intraband transitions, there are also indirect ones, in which an electron is scattered from $\mathbf{k}$ to $\mathbf{k}'$, but now these two states are not correlated directly with the phonon momentum $\mathbf{q}$ [7,46,51,58–61] [second term in Eq. (C7)]. This correlation is interrupted by the scattering of the electron on impurities or other quasiparticles in the system (e.g., other phonons). In our case, we only consider indirect transitions due to impurity scattering and we sum the leading terms of these processes. These terms are represented in Fig. 2(b), where the first two are the self-energy contributions, while the other two are the vertex corrections. This type of expansion is called high-energy (HE) expansion because it is valid for $\omega \gg |\varepsilon_{\mu\mathbf{k}} - \varepsilon_{\mu\mathbf{k}+\mathbf{q}}|$ [61].

Before performing the explicit summation of the diagrams in Fig. 2(b) we write the total phonon self-energy as the sum of direct and indirect terms:

$$\Pi_{\lambda}(\omega) = \Pi^{\text{d}}_{\lambda}(\omega) + \Pi^{\text{id}}_{\lambda}(\omega) \approx \pi^{\text{inter},0}_{\lambda}(\omega) + \pi^{\text{intra,HE}}_{\lambda}(\omega). \tag{36}$$

As for the interband transitions, we keep the leading direct contributions as in Eq. (22). The summation of the leading terms in $\pi^{\text{intra,HE}}_{\lambda}$ can be performed using the force-force correlation function approach for the phonon self-energy (see Appendix C and Refs. [49,55,61]):

$$\pi^{\text{intra,HE}}_{\lambda}(\omega) = -\frac{1}{\omega^2}[\phi_{\lambda\lambda}(\omega) - \phi_{\lambda\lambda}(0)]. \tag{37}$$

From the summation of the diagrams, we have

$$-\frac{\phi_{\lambda\lambda}(\omega)}{\omega^2} = -\frac{1}{\omega^2}\sum_{\mu\mathbf{k}\mathbf{k}'\sigma}\langle|V(\mathbf{k}-\mathbf{k}')|^2\rangle \times \left|g^{\mu\mu}_{\lambda}(\mathbf{k},0) + g^{\mu\mu}_{\lambda}(\mathbf{k}',0)\right|^2 \times \frac{f_{\mu\mathbf{k}} - f_{\mu\mathbf{k}'}}{\omega + \varepsilon_{\mu\mathbf{k}} - \varepsilon_{\mu\mathbf{k}'} + i\eta}, \tag{38}$$

where $\langle|V(\mathbf{k}-\mathbf{k}')|^2\rangle$ is the impurity potential averaged over impurity sites [55]. By combining Eqs. (37) and (38) we get that the high-energy expansion of the indirect contribution to the intraband phonon self-energy is

$$\pi_\lambda^{\text{intra,HE}}(\omega)=\sum_{\mu\mathbf{k}\sigma}\left|g_\lambda^{\mu\mu}(\mathbf{k},0)\right|^2\frac{\partial f_{\mu\mathbf{k}}}{\partial\varepsilon_{\mu\mathbf{k}}}\frac{\Delta\Sigma_{\mu\mu}^\lambda(\mathbf{k},\omega)}{\omega}. \quad (39)$$

In doing so, we have approximated the term $(f_{\mu\mathbf{k}}-f_{\mu\mathbf{k}'})/(\varepsilon_{\mu\mathbf{k}}-\varepsilon_{\mu\mathbf{k}'})$ with the derivative $\partial f_{\mu\mathbf{k}}/\partial\varepsilon_{\mu\mathbf{k}}$ to separate the $\mathbf{k}$ and $\mathbf{k}'$ summations. With this approximation the high-energy expansion of the intraband phonon self-energy acquires a form analogous to the high-energy expansion of the conductivity formula obtained within the memory-function model [49,53], the second-order Fermi golden rule formula [51], or the Holstein theory [51,82]. In Eq. (39) we have defined the *e-h* self-energy due to electron scattering on impurities as

$$\Delta\Sigma_{\mu\mu}^\lambda(\mathbf{k},\omega)=-\sum_{\mathbf{k}'}\langle|V(\mathbf{k}-\mathbf{k}')|^2\rangle\left(1-\frac{g_\lambda^{\mu\mu}(\mathbf{k}',0)}{g_\lambda^{\mu\mu}(\mathbf{k},0)}\right)\times\frac{2\omega}{(\omega+i\eta)^2+(\varepsilon_{\mu\mathbf{k}}-\varepsilon_{\mu\mathbf{k}'})^2}. \quad (40)$$

The relaxation processes described by the HE expansion term of Eq. (39) are of particular importance when the region of interest is far above the intraband Landau damping region ($\omega\gg|\varepsilon_{\mu\mathbf{k}}-\varepsilon_{\mu\mathbf{k}+\mathbf{q}}|$). Here we approximate the *e-h* self-energy $\Delta\Sigma_{\mu\mu}^\lambda(\mathbf{k},\omega)$ by the phenomenological parameter $i\Gamma_{\text{imp}}$,

$$\pi_\lambda^{\text{intra,HE}}(\omega)\approx i\sum_{\mu\mathbf{k}\sigma}\left|g_\lambda^{\mu\mu}(\mathbf{k},0)\right|^2\frac{\partial f_{\mu\mathbf{k}}}{\partial\varepsilon_{\mu\mathbf{k}}}\frac{\Gamma_{\text{imp}}}{\omega}. \quad (41)$$

From the structure of expressions (39)–(41) we can deduce that Γ_{imp} is actually the inverse of the transport relaxation time $\tau_{\text{tr}}^{\text{imp}}$ due to electron-impurity scattering obtained in the Boltzmann equations, i.e., $\Gamma_{\text{imp}}=1/\tau_{\text{tr}}^{\text{imp}}$ [55]. We note that the phenomenological damping energy $\Gamma_{\mu\mu}$ should in principle account for all relevant scattering processes in the system, while Γ_{imp} accounts just for the specific case of electron-impurity scattering. Using the above formalism, an equivalent expression for the indirect intraband phonon self-energy [Eq. (41)] can be derived for the case of electron-phonon scattering. In that case, a frequency- and temperature-dependent damping energy due to electron-phonon scattering $\Gamma_{\text{ph}}(\omega)$ appears instead of Γ_{imp} in Eq. (41) [6,47,55,57,83]. This damping energy contains information on which ($\mathbf{k}'-\mathbf{k}\neq 0,\lambda'$) phonon modes satisfying $\omega_{\mathbf{k}'-\mathbf{k},\lambda'}<\omega_{0\lambda}$ [47,51] are responsible for the damping of the studied ($\mathbf{q}\approx 0,\lambda$) phonon mode and the breakdown of the momentum conservation law. Contributions such as *e-h* pair dephasing [84] and indirect phonon-phonon coupling mediated by electron excitations [85], which are also important to describe the experimental phonon linewidth of a vibrating ordered layer of molecules on a metallic surface, are included in Eq. (41) with $\Gamma_{\text{ph}}(\omega)$. However, the corresponding analysis goes beyond the scope of the present work.

Finally, a further comment on the RTA form of the imaginary part of Eq. (23) is in order. Apart from the interband contribution, the RTA form of $\widehat{\pi}_\lambda^0(\omega)$ has an intraband contribution as well. The imaginary part of the former can be expressed as

$$-\text{Im}\widehat{\pi}_\lambda^{\text{intra},0}(\omega)\approx\frac{-\omega\Gamma_{\text{intra}}}{\omega^2+\Gamma_{\text{intra}}^2}\sum_{\mu\mathbf{k}\sigma}\left|g_\lambda^{\mu\mu}(\mathbf{k},0)\right|^2\frac{\partial f_{\mu\mathbf{k}}}{\partial\varepsilon_{\mu\mathbf{k}}}. \quad (42)$$

In the high-energy limit ($\omega\gg\Gamma_{\text{intra}}$) this expression is equivalent to the high-energy expansion of the intraband phonon self-energy $\pi_\lambda^{\text{intra,HE}}(\omega)$ [Eq. (41)] that we obtained by summation of the leading indirect terms in the electron-impurity scattering processes. However, there is no equivalent physical justification for the $\mathbf{q}\approx 0$ intraband transitions in Eq. (23) (Appendix A). Thus, this expression should be taken with caution if electron scattering processes are neglected and a finite (purely numerical) Γ_{intra} is used as a broadening parameter to simulate the clean noninteracting limit.

E. Quasistatic approximations for the phonon self-energy

A common practice when studying the linewidth of low-energy phonons and also of vibrationally excited adsorbates is the use of the quasistatic limit ($\omega_{0\lambda}\ll|\varepsilon_{\mu\mathbf{k}}-\varepsilon_{\mu'\mathbf{k}}|$) in Eqs. (10) and (17). In this respect, we consider it meaningful to examine step by step the implications of using this limit in calculations of the $\mathbf{q}\approx 0$ phonon self-energy. First of all, if the $\omega\to 0$ limit is taken directly in Eq. (10), the following expression is obtained:

$$\pi_\lambda^0(0)=\sum_{\mu\mu'\mathbf{k}\sigma}\frac{\left|d_\lambda^{\mu\mu'}(\mathbf{k},0)\right|^2}{2M_\lambda\omega_{0\lambda}}\frac{f_{\mu\mathbf{k}}-f_{\mu'\mathbf{k}}}{\varepsilon_{\mu\mathbf{k}}-\varepsilon_{\mu'\mathbf{k}}}, \quad (43)$$

where $d_\lambda^{\mu\mu'}(\mathbf{k},0)$ is the deformation potential defined in Eq. (4). This expression is purely real, which is actually required by the definition of the bare phonon self-energy given in Eq. (10). However, a practical formula for the phonon linewidth can still be obtained by taking carefully the quasistatic limit. In what follows we use η as a finite parameter, since this is usually done in DFT calculations to ensure numerical convergence. When applying the RTA as done above, a finite η is used, too, that has a physical meaning (i.e., $\eta=\Gamma_{\mu\mu'}$). We write the imaginary part of Eq. (10) for $\omega=\omega_{0\lambda}$ as

$$-\text{Im}\pi_\lambda^0(\omega_{0\lambda})=\pi\sum_{\mu\mu'\mathbf{k}\sigma}\frac{\left|d_\lambda^{\mu\mu'}(\mathbf{k},0)\right|^2}{2M_\lambda}\frac{f_{\mu\mathbf{k}}-f_{\mu'\mathbf{k}}}{\omega_{0\lambda}}\times\mathcal{L}_\eta(\omega_{0\lambda}+\varepsilon_{\mu\mathbf{k}}-\varepsilon_{\mu'\mathbf{k}}), \quad (44)$$

where $\mathcal{L}_\eta(x)$ stands for the Lorentzian function $\eta/\pi(x^2+\eta^2)$ (see Appendix D). To obtain the quasistatic limit that is always positive-definite we need to take the $\omega_{0\lambda}\to 0$ limit both in the Lorentzian function and in $(f_{\mu\mathbf{k}}-f_{\mu'\mathbf{k}})/\omega_{0\lambda}$. The latter limit is the derivative of the Fermi-Dirac distribution function, $-\partial f_{\mu\mathbf{k}}/\partial\varepsilon_{\mu\mathbf{k}}$. Otherwise, if we only took the limit of the Lorentzian function, the imaginary part could give negative, nonphysical values because it could happen that $f_{\mu\mathbf{k}}-f_{\mu'\mathbf{k}}<0$ when summation over the Fermi surface is performed. Therefore, by taking both limits the following expression for the quasistatic phonon self-energy is obtained:

$$-\text{Im}\pi_\lambda^0(0)\approx\pi\sum_{\mu\mu'\mathbf{k}\sigma}\frac{\left|d_\lambda^{\mu\mu'}(\mathbf{k},0)\right|^2}{2M_\lambda}\left(-\frac{\partial f_{\mu\mathbf{k}}}{\partial\varepsilon_{\mu\mathbf{k}}}\right)\times\mathcal{L}_\eta(\varepsilon_{\mu\mathbf{k}}-\varepsilon_{\mu'\mathbf{k}}). \quad (45)$$

In the low-temperature limit $T \to 0$, the derivative of the Fermi-Dirac distribution function $-\partial f_{\mu\mathbf{k}}/\partial\varepsilon_{\mu\mathbf{k}}$ goes to $\delta(\varepsilon_{\mu\mathbf{k}} - \varepsilon_F)$. This expression is also known as Allen's formula for the phonon linewidth [86]. The same formula can be obtained by taking the quasistatic limit in Eq. (17). In that case, the imaginary part for $\omega = \omega_{0\lambda}$ is

$$-\mathrm{Im}\widehat{\pi}^0_\lambda(\omega_{0\lambda}) = -\pi \sum_{\mu\mu'\mathbf{k}\sigma} \frac{\left|d^{\mu\mu'}_\lambda(\mathbf{k},0)\right|^2}{2M_\lambda} \frac{f_{\mu\mathbf{k}} - f_{\mu'\mathbf{k}}}{\varepsilon_{\mu\mathbf{k}} - \varepsilon_{\mu'\mathbf{k}}} \times \mathcal{L}_\eta(\omega_{0\lambda} + \varepsilon_{\mu\mathbf{k}} - \varepsilon_{\mu'\mathbf{k}}). \quad (46)$$

Since $-(f_{\mu\mathbf{k}} - f_{\mu'\mathbf{k}})/(\varepsilon_{\mu\mathbf{k}} - \varepsilon_{\mu'\mathbf{k}})$ is always positive, the $\omega_{0\lambda} \to 0$ limit in the Lorentzian function can be safely performed, which leads to the following quasistatic expression:

$$-\mathrm{Im}\widehat{\pi}^0_\lambda(0) \approx -\pi \sum_{\mu\mu'\mathbf{k}\sigma} \frac{\left|d^{\mu\mu'}_\lambda(\mathbf{k},0)\right|^2}{2M_\lambda} \frac{f_{\mu\mathbf{k}} - f_{\mu'\mathbf{k}}}{\varepsilon_{\mu\mathbf{k}} - \varepsilon_{\mu'\mathbf{k}}} \times \mathcal{L}_\eta(\varepsilon_{\mu\mathbf{k}} - \varepsilon_{\mu'\mathbf{k}}). \quad (47)$$

When we additionally require that $\varepsilon_{\mu\mathbf{k}} \to \varepsilon_{\mu'\mathbf{k}}$ this expression also leads to Allen's formula [Eq. (45)]. Since the intraband part of Allen's formula diverges [48], only the interband part is usually considered for calculating linewidths. To avoid this divergent form, the derivative $\partial/\partial\varepsilon_{\mu\mathbf{k}}$ can be applied to the Lorentzian $\mathcal{L}_\eta(x)$ instead of applying it to the Fermi-Dirac distribution function $f_{\mu\mathbf{k}}$ [35],

$$-\mathrm{Im}^\partial\pi^0_\lambda(0) \equiv -\pi \sum_{\mu\mu'\mathbf{k}\sigma} \frac{\left|d^{\mu\mu'}_\lambda(\mathbf{k},0)\right|^2}{2M_\lambda}(f_{\mu\mathbf{k}} - f_{\mu'\mathbf{k}}) \times \frac{\partial\mathcal{L}_\eta(\varepsilon_{\mu\mathbf{k}} - \varepsilon_{\mu'\mathbf{k}})}{\partial\varepsilon_{\mu\mathbf{k}}}. \quad (48)$$

Although this trick disregards the divergent intraband part, it actually changes the interband part as well, as we will explicitly show in the next section.

All in all, the expressions for the quasistatic $\mathbf{q} \approx 0$ phonon self-energies [Eqs. (45), (47), and (48)] should be taken with care when trying to simulate the clean noninteracting limit $\eta \to 0^+$, for which the imaginary part should vanish by definition (adiabaticity), as Eq. (43) shows. Nevertheless, if the physically relevant transitions occur mostly at the Fermi surface, as happens for the $\omega_{0\lambda} \to 0$ limit (e.g., small phonon frequencies, acoustic phonons), Eqs. (45) and (47) imply that a finite η could be useful. However, note that the strict $\eta \to 0^+$ limit in these expressions is nonphysical because it leads to divergent values [87]. Furthermore, too large η values in the RTA could also give nonphysical values, since it could happen that Eqs. (45) and (47) account for inelastic interband transitions when $\eta \gtrsim \omega_{0\lambda}$, although these expressions suggest that only the quasielastic transitions at the Fermi surface should contribute. A similar precaution should be taken when studying the quasistatic limit for low-frequency $\mathbf{q} \neq 0$ modes (e.g., adiabatic electronic friction coefficient) [32,34,36,37]. In that case Allen's formula should be more reliable, since the intraband part is not divergent for finite $\mathbf{q}$ [48].

III. THE CASE OF CO STRETCH MODE ON THE Cu(100) SURFACE

A. Computational details

All calculations were done using the plane-wave DFT-based QUANTUM ESPRESSO (QE) package [88] with a plane-wave cutoff energy of 50 Ry. The core-electron interaction was approximated with ultrasoft pseudopotentials, and the exchange and correlation functional with the revPBE version [89] of the generalized gradient approximation (GGA) [90]. The adiabatic vibrational frequencies $\omega_{0\lambda}$ and harmonic electron-phonon matrix elements $g^{\mu\mu'}_\lambda(\mathbf{k},0)$ defined in Eq. (4) were calculated on a $(8 \times 8 \times 1)$ Monkhorst-Pack $\mathbf{k}$ point grid [91] using density functional perturbation theory (DFPT) [3]. In that case, $\psi_{\mu\mathbf{k}}$ are the Kohn-Sham (KS) electronic wave functions, while V_{ei} is replaced with the self-consistent KS potential V^{SCF} in both electron-phonon matrix elements. Generally, the KS potential is frequency dependent. However, for practical reasons it is approximated with its static value $V^{SCF} \approx V^{SCF}(\omega = 0)$ in usual DFT calculations [70,79]. In order to calculate the different phonon self-energies discussed in Sec. II we use denser $\mathbf{k}$ point grids ranging from $(16 \times 16 \times 1)$ to $(160 \times 160 \times 1)$. In doing so, the electron-phonon matrix elements $g^{\mu\mu'}_\lambda(\mathbf{k},0)$ obtained on the coarser grid are interpolated on these denser grids following the QE implementation.

B. Geometric and electronic structure

All the analysis is performed for the adsorption structure and coverage reported from IRAS experiments in Ref. [64]: one CO molecule in the $c(2 \times 2)$ unit cell of Cu(100) adsorbed vertically on the top site [Fig. 3(a)]. Using the aforementioned parameters, the adsorption geometry is optimized until forces are smaller than 0.01 eV/Å, where only the bottom surface layer is not allowed to move. The obtained Cu-C and C-O bond lengths are 1.875 and 1.154 Å, respectively, which are in good agreement with the experimental data [92] and previous theoretical works [93]. In our study we vary the number of Cu layers, going from three to 18 layers. Although the relevant geometrical parameters (Cu-C and C-O bond lengths) do not depend much on the number of layers included in the calculation, we will show how it significantly affects the electronic structure and, hence, the calculated phonon linewidth.

Obviously, the perturbation induced by the CO stretch mode is so localized in the molecule that it will overall affect the electronic states that consist of a mixture of CO and Cu states. It is for these states that the matrix elements $g^{\mu\mu'}_\lambda(\mathbf{k},0)$ may take finite non-negligible values. The projected density of states (PDOS) and the electronic band structure along the the high-symmetry points of the Brillouin zone allow us to identify the states contributing to the finite phonon linewidth (the PDOS is calculated by projecting on s and p states centered at the selected atoms, using the implementation of QE). The results for the CO/Cu(100) system with three layers are shown in Fig. 3(b). The color scale in the band structure represents states contributed by either the CO molecule (red color) or Cu atoms (purple color). This identification was made by defining

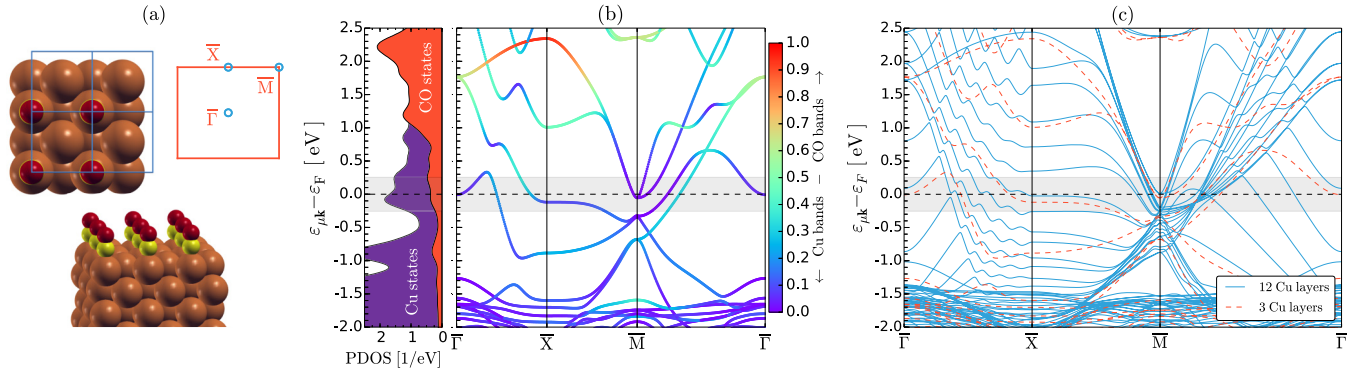

FIG. 3. (a) Unit cell of the $c(2 \times 2)$ structure of CO molecules adsorbed on the top site of the Cu(100) surface and the corresponding Brillouin zone with high-symmetry points. Red balls represent oxygen, yellow ones carbon, and brown ones copper atoms. (b) The electronic band structure for the CO molecule on the Cu(100) three-layer surface. Red (purple) bands correspond to contributions from the CO molecule (Cu atoms). Additionally, the projected density of states is shown for CO (red) and Cu (purple) states. (c) Comparison between the electronic band structure of CO adsorbed on 12 (blue lines) and three (red dashed lines) layers of the Cu(100) surface. The shaded areas in the electronic band plots represent the energy window $\varepsilon_F \pm \omega_{0\lambda}$, where $\omega_{0\lambda}$ is the energy of the CO stretch mode.

the coefficient $\mathcal{C}_{\mu\mathbf{k}}$ for each state as

$$\mathcal{C}_{\mu\mathbf{k}} = \frac{\iint dxdy \int_{z_0-a}^{z_0+a} dz |\psi_{\mu\mathbf{k}}(\mathbf{r})|^2}{\int_V d\mathbf{r} |\psi_{\mu\mathbf{k}}(\mathbf{r})|^2}, \tag{49}$$

where a is the distance between the midpoint of CO and the midpoint of the Cu-C bond, z_0 is the z coordinate of the midpoint of CO, and V is the total volume of the unit cell.

In agreement with Refs. [34,93], the PDOS shows that there is a significant hybridization between the CO states with p symmetry (π^*) and the Cu states around the Fermi level. In addition, the colored band structure provides precise information on what states can contribute to the interband transition with $\mathbf{q} \approx 0$. Note that only electronic transitions within the shaded gray area around the Fermi energy can be induced by the CO stretch mode ($\omega_{0\lambda}^{\text{exp}} = 0.259$ eV [15]). Clearly, this region is poorly described by the three-layer surface. However, as we increase the number of Cu layers, the number of bands in this area increases significantly [Fig. 3(c)]. Therefore, it is reasonable to expect that the imaginary part of any of the above phonon self-energy expressions changes with the increase of the number of electronic bands, since more electronic transitions fulfilling the energy conservation condition $\delta(\omega_{0\lambda} + \varepsilon_{\mu\mathbf{k}} - \varepsilon_{\mu'\mathbf{k}})$ may contribute to the matrix elements $g_\lambda^{\mu\mu'}$ defined by Eq. (4). As dictated by the causality principle, the real part of the phonon self-energy can be obtained by using the imaginary part and the Kramers-Kronig relations, so the mentioned changes will affect the real part as well. All these observations indicate that a proper description of the Cu surface is needed to assure an accurate calculation of the phonon self-energy.

C. Phonon linewidth

Before analyzing the role of electronic relaxation processes in the stretch mode linewidth of CO adsorbed on Cu(100), it is necessary to assure first that the value of the noninteracting phonon linewidth is well converged with respect to those parameters controlling the quality of the CO/Cu(100) electronic states, namely, the number of $\mathbf{k}$ points and the number of Cu layers. In doing this selection, one should be aware that the Dirac delta function appearing in the imaginary part of Eq. (10) (bare phonon self-energy) is numerically approximated by a Lorentzian function of half-width at half-maximum η. Therefore, the calculated values of the bare phonon linewidth should be well converged for reasonably small η values as we check next.

In an ideal situation, the summation appearing in the expressions of correlation functions (e.g., phonon self-energy) would be a continuous integral over the $\mathbf{k}$ space. Thus, in order to obtain accurate numerical results, we need to achieve convergence with respect to the discrete number of $\mathbf{k}$ points used to simulate the continuum. To clarify this issue we plot in Fig. 4 the results for the CO stretch mode phonon linewidth obtained with Eq. (10) as a function of η and for different $\mathbf{k}$ point grids, where all the calculations were performed for a slab of six Cu layers. We observe that for $\eta \geqslant 60$ meV the convergence is achieved with the $(48 \times 48 \times 1)$ grid, while for smaller values of η we need at least the $(72 \times 72 \times 1)$ grid.

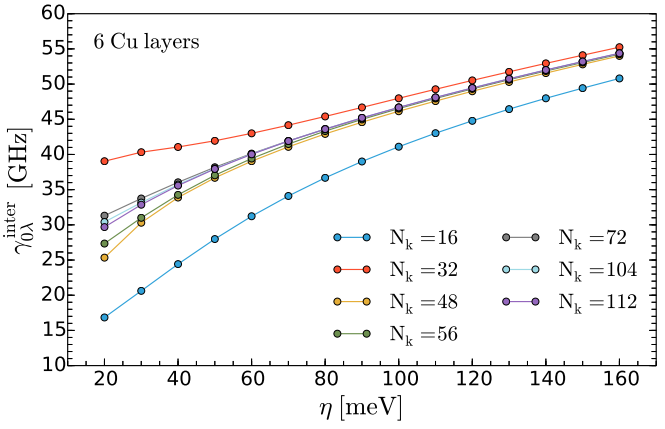

FIG. 4. Interband part of the $\mathbf{q} \approx 0$ phonon linewidth $\gamma_{0\lambda}^{\text{inter}}$ of the CO stretch mode as a function of η calculated with Eq. (10). The Cu(100) surface is approximated by six layers. The number N_k defines the $\mathbf{k}$ point grid with $(N_k \times N_k \times 1)$. The temperature is $T = 200$ K.

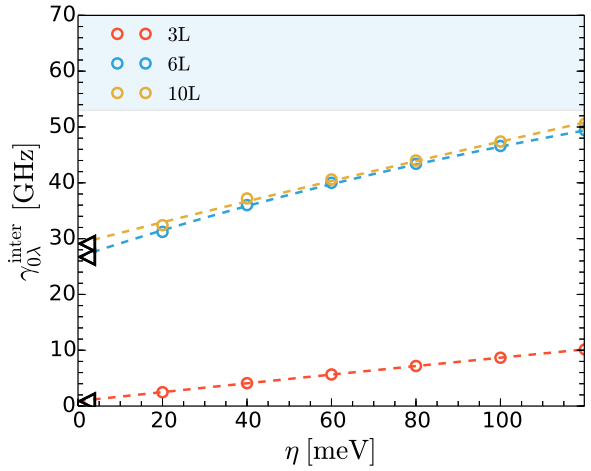

FIG. 5. Interband part of the $\mathbf{q} \approx 0$ phonon linewidth $\gamma_{0\lambda}^{\rm inter}$ of the CO stretch mode on the Cu(100) surface for three, six, and 10 Cu layers (red, blue, and yellow colors, respectively). The results are obtained with Eq. (10) and extrapolating the finite η values to $\eta = 0$ to get the result of the bare phonon linewidth (black triangles). The number of $\mathbf{k}$ points used here is $(160 \times 160 \times 1)$ for three layers, and $(72 \times 72 \times 1)$ for six and 10 layers. The temperature is $T = 200$ K. The blue shaded area represents the area from the lowest measured experimental linewidth (∼50 GHz) to the highest one (∼140 GHz) (including experimental error bars).

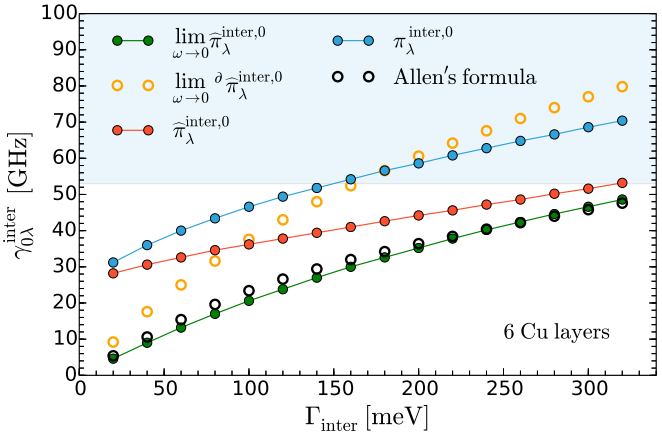

FIG. 6. Interband part of the $\mathbf{q} \approx 0$ phonon linewidth $\gamma_{0\lambda}^{\rm inter}$ of the CO stretch mode as a function of $\Gamma_{\rm inter}$ for six Cu layers calculated with Eqs. (22) (blue circles), (23) (red circles), (45) (black circles), (47) (green circles), and (48) (yellow circles), using the $(72 \times 72 \times 1)$ $\mathbf{k}$ point grid. Blue shaded area as in Fig. 5. The temperature is $T = 200$ K.

Therefore, this latter grid will be used in the rest of this section unless otherwise stated.

The convergence of the bare phonon self-energy as a function of the number of Cu layers used in the slab is shown in Fig. 5. For each slab, the phonon linewidth in the clean noninteracting limit $\eta \to 0^+$ (black triangles) is obtained by extrapolating the corresponding $\gamma_{0\lambda}^{\rm inter}(\eta)$ curve. The results of Fig. 5 show that the bare $\gamma_{0\lambda}^{\rm inter}$ obtained with six Cu layers is already converged. Importantly, the obtained values for six and 10 layers are 26.7 and 29.1 GHz, respectively, which are far beneath the lowest reported experimental values [15,64,65,67]. In principle, a theoretical linewidth smaller than the experimental one is not that surprising, because further electron scattering effects that exist under real experimental conditions are not captured by an ideal theoretical model. For this reason we analyze next how these results change when electron relaxation processes are included at the RTA level ($\eta \to \Gamma_{\rm inter}$), i.e., by giving a physical meaning to the broadening.

The results in Fig. 6 show the values of $\gamma_{0\lambda}^{\rm inter}$ for six Cu layers as a function of the damping energy $\Gamma_{\rm inter}$ calculated with the RTA phonon self-energy $\pi_\lambda^{\rm inter,0}(\omega_{0\lambda})$ [see Eq. (22)]. We observe how the phonon linewidth increases with the damping energy, i.e., with the intensity of the electronic scattering processes. Consequently, including a finite electron damping energy improves the bare phonon linewidth result by bringing it closer to the experimental values. Figure 6 also shows that the results obtained with $\pi_\lambda^{\rm inter,0}(\omega_{0\lambda})$ [Eq. (22)] (blue circles) and $\widehat{\pi}_\lambda^{\rm inter,0}(\omega_{0\lambda})$ [Eq. (23)] (red circles) are different for finite $\Gamma_{\rm inter}$, while they tend to the same values when $\Gamma_{\rm inter} \to 0^+$. Note that, as discussed in Sec. II (see also Appendix D), Eq. (22) is the correct phonon self-energy within the RTA. This shows that Eq. (23), which corresponds to introducing a finite damping into the phonon self-energy expression obtained after removing the adiabatic contribution [Eq. (17)], is only correct in the strict $\Gamma_{\rm inter} \to 0$ limit, but not in the general RTA with finite $\Gamma_{\rm inter}$.

In order to get insight in the limitations of the quasistatic limit for high-frequency vibrational modes or for optical phonons, we also show in Fig. 6 the quasistatic forms of the interband phonon linewidths obtained with Allen's formula [Eq. (45)] (black circles), $\widehat{\pi}_\lambda^{\rm inter,0}(0)$ [Eq. (47)] (green circles), and ${}^{\partial}\pi_\lambda^{\rm inter,0}(0)$ [Eq. (48)] (yellow circles). Recall here that Eq. (47) is obtained by taking the quasistatic limit in Eq. (23) (as described in Sec. II E) when $\eta \to \Gamma_{\rm inter}$. Allen's formula is obtained after taking $\omega_{0\lambda} \to 0$ and $\varepsilon_{\mu\mathbf{k}} \to \varepsilon_{\mu'\mathbf{k}}$ in Eqs. (44) and (47), respectively. Additionally, Eq. (48) has been used in the literature to avoid the divergence in the intraband part of the phonon self-energy in the quasistatic limit [35]. As $\Gamma_{\rm inter} \to 0^+$ the three quasistatic curves go to zero, as required by definition of adiabaticity. For large values of $\Gamma_{\rm inter}$ the phonon linewidth obtained with $\widehat{\pi}_\lambda^{\rm inter,0}(0)$ approaches the result obtained with $\widehat{\pi}_\lambda^{\rm inter,0}(\omega_{0\lambda})$, which means that the proper resolution in the Lorentzian is lost when $\Gamma_{\rm inter}$ becomes larger than $\omega_{0\lambda}$. From the perspective of the quasistatic expression $\widehat{\pi}_\lambda^{\rm inter,0}(0)$ this implies that $\Gamma_{\rm inter}$ is so large that it actually introduces dynamic ($\omega \neq 0$) instead of static contributions, which are the only ones that should strictly appear in the quasistatic limit. Similarly, the large broadening parameter ($\eta = 0.6$ eV) used in Ref. [41] forces the quasistatic phonon linewidth, and also the adiabatic friction coefficients that are calculated from an expression analogous to $\widehat{\pi}_\lambda^{\rm inter,0}(0)$, to fall into the dynamical regime. In a realistic situation the case $\Gamma_{\rm inter} \gtrsim \omega_{0\lambda}$ is unlikely to happen, because the energy of the CO stretch mode is 0.26 eV, and a value $\Gamma_{\rm inter} \gtrsim 0.26$ eV would correspond to a very dirty system characterized by various and highly probable scattering processes. In fact, the realistic values of $\Gamma_{\rm inter}$ should be within the same order of magnitude as $\Gamma_{\rm intra}$ [54,94], where the usual values range from ∼1 meV

up to around 100 meV [95]. Therefore the values of $\gamma_{0\lambda}^{\text{inter}}$ at $\Gamma_{\text{inter}} \approx 100$–$150$ meV should be taken as the uppermost limit. The results obtained from the interband part of Allen's formula (black circles) exhibit a dependence on Γ_{inter} very similar to that of the interband phonon linewidth obtained from Eq. (47). Regarding the results of the phonon linewidth obtained with ${}^{\partial}\pi_{\lambda}^{\text{inter},0}(0)$, note that even if they match the $\pi_{\lambda}^{\text{inter},0}(\omega_{0\lambda})$ results for some values of Γ_{inter}, this quasistatic limit faces the same inconsistencies as $\widehat{\pi}_{\lambda}^{\text{inter},0}(0)$ for $\Gamma_{\text{inter}} \lesssim 150$ meV.

Having the above discussion in mind, we can summarize the problems of the quasistatic approximations when applied to high-frequency modes in the following two points: (i) if the clean noninteracting limit ($\Gamma_{\text{inter}} \to 0^{+}$) is simulated, then the interband expressions in the quasistatic limit are zero, leaving only the intraband term of $\widehat{\pi}_{\lambda}^{0}(0)$ finite (as discussed in Sec. II E). (ii) If the interacting case ($\Gamma_{\text{inter}} > 0$) is regarded relevant in the studied system, then realistic values of Γ_{inter} should be taken into account, since the phonon linewidth is not constant with respect to different Γ_{inter} values. However, even in that case the quasistatic approximations may give inconsistent results, being therefore more meaningful to use the frequency-dependent phonon self-energy $\pi_{\lambda}^{\text{inter},0}(\omega_{0\lambda})$.

As for the temperature effects that enter the Fermi-Dirac distribution functions $f_{\mu\mathbf{k}}$, we observe only minor changes in the phonon linewidth. Specifically, $\gamma_{0\lambda}^{\text{inter}}$ changes less than 1 GHz for electronic temperatures within the range $T = 40$–300 K. In general, this does not mean that the phonon linewidth due to electron-phonon coupling is independent of temperature. Well on the contrary, the *e-h* self-energy is a complex function of temperature, and thus the damping energy Γ_{inter} should also change when the temperature changes (in a way similar to that in which Γ_{intra} changes in Refs. [6,7,47,57]).

Next we analyze the effect of including electronic relaxation processes in the electron distribution functions, i.e., of replacing $f_{\mu\mathbf{k}}$ by $n_{\mu}(\mathbf{k})$ as defined in Eq. (27). The results for this replacement are shown in Fig. 7 for three different values of Γ^{A}. For each Γ_{inter}, the interband phonon linewidth increases when including relaxation processes in the distribution function. As a result we get better agreement with the experimental values. Still, it is not possible to establish a correct quantitative estimation of the theoretical $\gamma_{0\lambda}^{\text{inter}}$ since the exact value of Γ^{A} is unknown, except for the fact that it should be within the usual values of the electron self-energy ($\sim$1–100 meV). Thus these results show qualitatively how accounting for relaxation processes in the single-electron spectral function (quasiparticle linewidth) influences the phonon linewidth through the momentum distribution function.

So far we have only considered the interband transitions without paying attention to the intraband ones, which are proportional to q^{2} and thus negligible for the $\mathbf{q} \approx 0$ optical phonons, i.e., the CO stretch mode in our particular case. If we take into account higher-order electron scattering processes (e.g., electron-impurity scattering), the indirect intraband channel is open, as discussed in Sec. II D. For the CO stretch mode excited by infrared light ($\mathbf{q} \approx 0$), the condition $\omega \gg |\varepsilon_{\mu\mathbf{k}} - \varepsilon_{\mu\mathbf{k}+\mathbf{q}}|$ is met. Thus we can apply the high-energy expansion of the indirect intraband phonon self-energy provided by Eq. (41). The corresponding values of $-\text{Im}\pi_{\lambda}^{\text{intra,HE}}(\omega_{0\lambda})$ are shown in Fig. 8 as a function

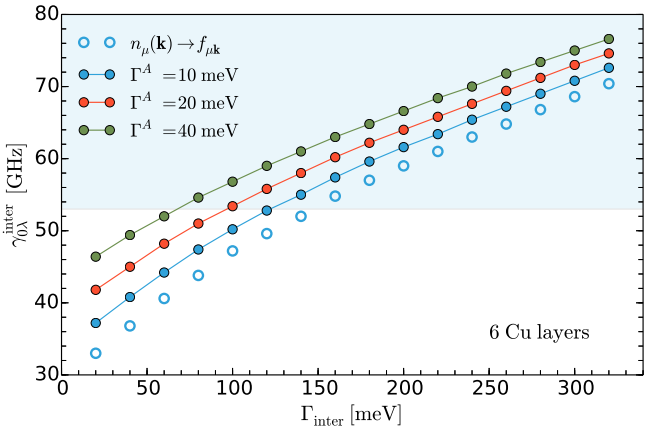

FIG. 7. $\gamma_{0\lambda}^{\text{inter}}$ as a function of Γ_{inter} of the CO stretch mode obtained with Eq. (24), where the low-temperature ($T = 10$ K) Fermi-Dirac distribution functions $f_{\mu\mathbf{k}}$ (open circles) are replaced with the momentum distribution functions $n_{\mu}(\mathbf{k})$ obtained with Eq. (27) (closed circles). The results are shown also for different damping energies of the single-particle spectral function Γ^{A}. The number of $\mathbf{k}$ points used here is $(72 \times 72 \times 1)$. Blue shaded area as in Fig. 5.

of Γ_{imp}. As the intraband damping energies (i.e., transport relaxation times, τ_{tr}) can be extracted very easily from optical conductivity measurements by fitting the results to the Drude model, the values for usual bulk systems are well known. The reported values for bulk Cu in the range $T = 60$–150 K are $1/\tau_{\text{tr}} = 2$–11 meV [95]. Applying these values to our system we get $-\text{Im}\pi_{\lambda}^{\text{intra,HE}}(\omega_{0\lambda}) \approx 10$–$30$ GHz (Fig. 8). Note however that this value should be taken as a rough estimation, since the intraband electron scattering processes in bulk Cu could be different from the ones in CO/Cu(100). Moreover, $1/\tau_{\text{tr}}$ is the total transport relaxation time accounting for all the relevant scattering processes in the system ($1/\tau_{\text{tr}} = 1/\tau_{\text{tr}}^{\text{imp}} + 1/\tau_{\text{tr}}^{\text{ph}} + 1/\tau_{\text{tr}}^{\text{el}}$, where $\tau_{\text{tr}}^{\text{imp}}$, $\tau_{\text{tr}}^{\text{ph}}$, and $\tau_{\text{tr}}^{\text{el}}$ are the relaxation times

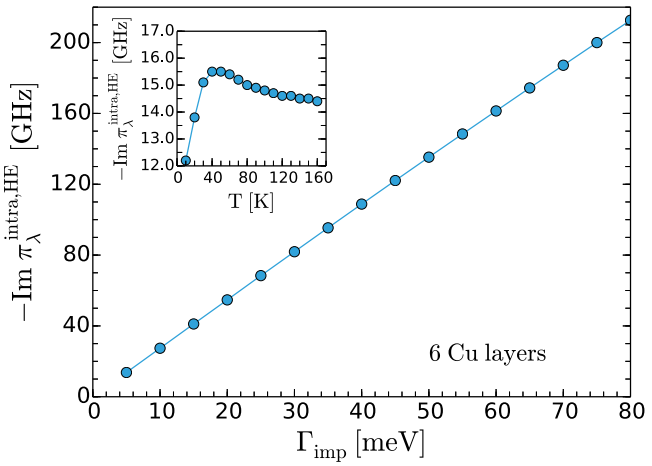

FIG. 8. High-energy expansion of the indirect contribution to the intraband phonon self-energy [Eq. (41)] of the CO stretch mode as a function of Γ_{imp} with $T = 200$ K and as a function of the temperature with $\Gamma_{\text{imp}} = 5$ meV (inset) for six Cu layers. The number of $\mathbf{k}$ points used here is $(80 \times 80 \times 1)$.

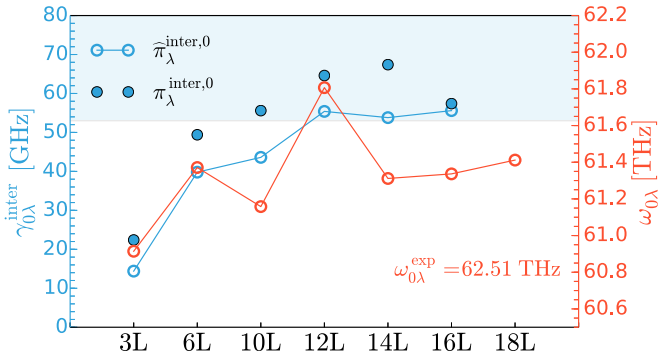

FIG. 9. $\gamma_{0\lambda}^{\text{inter}}$ of the CO stretch mode calculated with Eqs. (22) (blue circles) and (23) (open blue circles), and the long-wavelength adiabatic frequency of the CO stretch mode, $\omega_{0\lambda}$ (open red circles), as a function of the number of Cu layers. The damping energy is $\Gamma_{\text{inter}} = 150$ meV and the numbers of $\mathbf{k}$ points are $N_k = 160,72,72,56,56,32$ for the number of layers $N_{\text{layer}} = 3,6,10,12,14,16$, respectively. Blue shaded area as in Fig. 5. The temperature is $T = 200$ K.

for impurity, phonon, and electron scattering, respectively) and not just for electron-impurity scattering ($1/\tau_{\text{tr}}^{\text{imp}}$). In the inset of Fig. 8 we also show the temperature dependence of $-\text{Im}\pi_\lambda^{\text{intra,HE}}(\omega_{0\lambda})$ obtained through the $\partial f_{\mu\mathbf{k}}/\partial\varepsilon_{\mu\mathbf{k}}$ factor. In the range $T = 100$–160 K relevant for the experiment [65], no significant temperature effects are observed.

As we mentioned earlier, the calculated phonon linewidth depends on the number of Cu layers used to describe the surface. In Fig. 9 we show the RTA phonon linewidth $\gamma_{0\lambda}^{\text{inter}}$ obtained with Eqs. (22) (open blue circles) and (23) (blue circles) as a function of the number of Cu layers. As we already anticipated from the electronic structure analysis in Sec. III B, the RTA linewidths are closer to the experimental values as the slab thickness increases from three to 16 layers. Here we see that six layers provide a reasonably good approximation for the surface and, even though the linewidth further increases with the number of layers, the change is not drastic. Also, the RTA phonon linewidths obtained with $\pi_\lambda^{\text{inter},0}(\omega_{0\lambda})$ are always higher than the ones obtained with $\widehat{\pi}_\lambda^{\text{inter},0}(\omega_{0\lambda})$. The presented results are calculated with $\Gamma_{\text{inter}} = 150$ meV, so they should be interpreted as an upper limit for the given number of Cu layers.

To get a more precise estimation of the RTA phonon linewidths and the corresponding phenomenological damping energies (e.g., Γ_{inter}, Γ^A, and Γ_{imp}), one should either calculate the damping energies $\text{Im}\Sigma_\mu(\mathbf{k},\varepsilon)$ and $\text{Im}\Delta\Sigma_{\mu\mu'}(\mathbf{k},\mathbf{q},\omega)$ explicitly [53], or extract these values from experiments, for example angle-resolved photoemission spectroscopy (ARPES) for the former and optical conductivity measurements for the latter. These calculations are rather difficult to do *ab initio*, and according to our knowledge, this has not been done yet systematically for both intraband and interband phonon self-energies. As for experiments, they are not available for our studied system. Thus, we are restricted to phenomenological calculations, where we give the results for a range of meaningful damping energies Γ.

TABLE I. Renormalization of the CO stretch mode frequency on the Cu(100) surface ($\omega_{0\lambda} = 61.37$ THz) due to the nonadiabatic electron-phonon coupling. The number of Cu layers is six and the $\mathbf{k}$ point grid is ($80 \times 80 \times 1$). The units are THz.

	$\mathbf{q} \approx 0$					
	intraband		interband		total	
	π_λ^0	$\widehat{\pi}_\lambda^0$	π_λ^0	$\widehat{\pi}_\lambda^0$	π_λ^0	$\widehat{\pi}_\lambda^0$
$\text{Re}\pi_\lambda^0$	0.0	0.69	−4.97	−0.019	−4.97	0.671
$\omega_{0\lambda} + \text{Re}\pi_\lambda^0$	61.37	62.06	56.4	61.35	56.4	62.04
$\omega_{0\lambda}^{\text{exp}}$ [15]						62.51

D. Renormalization of the phonon frequency

If the change from the adiabatic to the nonadiabatic phonon frequency is relatively small, the renormalization of the $\mathbf{q} \approx 0$ phonon frequencies given by Eq. (8) can be approximated as

$$\omega^{\text{NA}} \approx \omega_{0\lambda} + \text{Re}\pi_\lambda^0(\omega_{0\lambda}), \tag{50}$$

where we have changed the exact form of the phonon self-energy by the bare one, and $\omega_{0\lambda}$ is the phonon frequency obtained within the adiabatic DFT calculations (see Appendix A). For the CO stretch mode we get $\omega_{0\lambda} \simeq 61.4$ THz as the converged value (see Fig. 9, right y axis), which is already in good agreement with the reported experimental value $\omega_{0\lambda}^{\text{exp}} = 62.51$ THz [15]. This means that nonadiabatic effects should indeed be small as we demonstrate next.

Table I shows the results for the real parts of $\widehat{\pi}_\lambda^0(\omega_{0\lambda})$ [Eqs. (19) and (21)] calculated with six Cu layers, as well as the corresponding nonadiabatic phonon frequencies ω^{NA}. For completeness, we have also calculated the interband part of $\text{Re}\pi_\lambda^0(\omega_{0\lambda})$ [Eq. (15)], although it cannot be taken as a correction to the DFT adiabatic frequency (see Sec. II A). Note that it actually would reduce the value of $\omega_{0\lambda}$, and therefore further increase the difference between calculated and experimental frequencies. On the contrary, the phonon self-energy $\widehat{\pi}_\lambda^0(\omega_{0\lambda})$, which directly gives the difference between the adiabatic and nonadiabatic frequencies [5,10,75] (see Sec. II A), shifts the phonon frequency closer to the experimental one. The next point we investigate is how sensitive this value is to the number of Cu layers used in the calculation.

Figure 10 shows the intraband and interband contributions to $\text{Re}\widehat{\pi}_\lambda^0(\omega_{0\lambda})$ as a function of the number of Cu layers. The interband contribution is in all cases very small, so it does not affect the phonon frequency. However, the converged value of the intraband part is between 2 and 2.5 THz. With this value the nonadiabatic frequency overestimates the experimental value by around 1 THz. Although the accuracy could be improved by choosing a finite η as in the inset of Fig. 10 (electronic damping effects as in Ref. [10]) or possibly by the long-range screening effects discussed in Sec. II C, we leave the results as they are for at least three reasons: (i) all the above nonadiabatic corrections to the phonon frequencies are relatively small, (ii) the adiabatic phonon frequency $\omega_{0\lambda}$ could depend on the choice of the DFT functional [96], and (iii) there is no way to our knowledge to use $\widehat{\pi}_\lambda^0(\omega)$ in a diagrammatic perturbation expansion to obtain the electronic damping effects. One

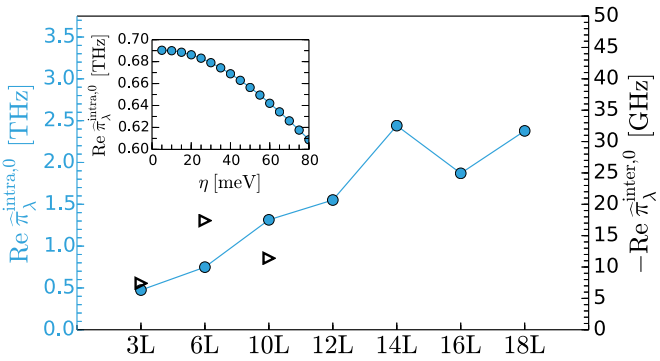

FIG. 10. Real part of the intraband (blue circles) [Eq. (19)] and interband (black triangles) [Eq. (21)] contributions to the phonon self-energy $\widehat{\pi}_\lambda^0(\omega_{0\lambda})$ of the CO stretch mode as a function of the number of Cu layers. The numbers of $\mathbf{k}$ points used are $N_k = 160{,}80$ for $N_{\text{layer}} = 3{,}6$ and $N_k = 64$ for the rest. The inset shows the intraband contribution Eq. (19) for six Cu layers as a function of η, where the $\eta \to 0^+$ limit corresponds to the results presented in the main panel.

possibility for (iii) would be not to use $\widehat{\pi}_\lambda^0(\omega)$ directly, but to gather all the irreducible diagram terms in a random phase approximation fashion for $\pi_\lambda^0(\omega)$, and then subtract the static part in the clean noninteracting limit from the dynamic one, $\Pi_\lambda(\omega) - \pi_\lambda^0(0)$ (this is precisely explored in Appendix B). For the indirect intraband channel this summation of diagrams would include all possible scattering processes beyond the leading terms presented in Fig. 2(b), which would lead to a phonon self-energy not just valid for $\omega \gg |\varepsilon_{\mu\mathbf{k}} - \varepsilon_{\mu\mathbf{k}+\mathbf{q}}|$, but for any ω value [61]. This goes beyond the scope of the present work.

IV. CONCLUSION

We have analyzed the dynamical (nonadiabatic) phonon self-energy in the long-wavelength limit, both for cases where electronic scattering processes are disregarded and where they are included in a phenomenological way (relaxation-time approximation). This general formulation was then used to calculate the long-wavelength phonon linewidth and frequency shift due to the electron-phonon coupling for the CO stretch mode on the Cu(100) surface.

The results for the phonon linewidth show that the phonon self-energy in the clean noninteracting limit, corresponding to the first-order Fermi golden rule formula, is not enough to explain the experimental results of the CO stretch mode obtained from infrared spectroscopy. To get a better agreement it is necessary to account for electronic scattering processes (i.e., electron scattering on phonons, impurities, or other electrons). We do so by including a finite electron self-energy into the Green's functions and use them together with the Dyson equation to construct the phonon self-energy. This procedure naturally includes electron damping processes in the phonon self-energy through the difference of electron and hole self-energies, as well as through the single-electron spectral function that enters the momentum distribution functions. Using a phenomenological treatment we have shown that this phonon self-energy (mostly the imaginary part) is then considerably affected by the mentioned scattering processes, that is, by the corresponding damping energies. For electron-impurity scattering processes we have summed the four leading terms in the high-energy expansion of the indirect contribution to the intraband phonon self-energy. The result gives us an expression for the phonon self-energy analogous to the high-energy form of the intraband Kubo conductivity formula, and we obtain the explicit expression for the *e-h* self-energy, which resembles the inverse of the transport relaxation time caused by electron-impurity scattering. Since the contamination with impurities is unavoidable in the experimental setup, the high-energy indirect phonon self-energy term, together with the relaxation-time approximation of the direct interband phonon self-energy, is relevant for explaining the experimental phonon linewidths. Along with these two contributions, it is expected that electron-hole pair dephasing [84] and indirect phonon-phonon coupling mediated by electron excitations [7,47,85], as well as the improvement of semilocal DFT functionals, should contribute to improve the agreement with the experimental linewidth. Further work along the latter three contributions would be desirable.

We have examined in addition the reliability of the quasistatic approximation for the phonon linewidth of the CO stretch mode. Considerably different results with respect to the dynamical phonon linewidth are found, especially for damping energies that are much smaller than the phonon frequency of the CO stretch mode (0.26 eV). Importantly, we have shown that the interband part of the $\mathbf{q} = 0$ quasistatic phonon self-energy is exactly zero in the limit of zero damping energy. For this reason, the quantity that is calculated using this approach with finite damping values [41] cannot be connected to the adiabatic friction coefficient of atoms/molecules interacting with metal surfaces because it already includes dynamical effects that should be absent from it. Quasistatic expressions are expected to show the same flaws for similar high-frequency modes in other systems when $\mathbf{q} = 0$. Therefore, Allen's formula (both its intraband and interband parts) is not applicable when calculating the phonon linewidth of high-frequency modes obtained in infrared or Raman spectroscopies [48]. Nevertheless, we expect it to be suitable for low-frequency modes and for $\mathbf{q} \neq 0$.

We have also found that the temperature dependence of the phonon linewidth that comes from the Fermi-Dirac distribution function is negligible. However, electronic scattering processes (i.e., electron self-energy) are also temperature dependent and they are expected to affect the overall temperature dependence of the phonon self-energy. Regarding the renormalization of the CO stretch mode, we have shown the necessity of subtracting the static (adiabatic) phonon self-energy from the dynamic (nonadiabatic) one. The result so obtained is more reasonable, since adiabaticity is already included in the phonon frequency obtained from DFT-based calculations. In addition, we have found that the phonon linewidth is very sensitive to the parameters used. Good convergence is only achieved after a careful consideration of the numbers of $\mathbf{k}$ points and surface layers.

Finally, we would like to emphasize that the present approach to study nonadiabatic effects is a general one and can be applied for any well-defined high-energy optical phonon mode.

ACKNOWLEDGMENTS

Useful discussions with I. Kupčić (University of Zagreb) are gratefully acknowledged. This work has been supported by the Basque Departamento de Educación, Universidades, e Investigación, the University of the Basque Country UPV/EHU (Grant No. IT-756-13), and the Spanish Ministerio de Economía y Competitividad (Grant No. FIS2013-48286-C2-2-P). Computational resources were provided by the DIPC computing center.

APPENDIX A: NONADIABATIC EFFECTS IN THE ELECTRON-ION SYSTEM

Here we briefly summarize the two approaches to derive the bare phonon self-energy due to the electron-phonon coupling (a) when the goal is to calculate the adiabatic ($\omega = 0$) and nonadiabatic ($\omega \neq 0$) effects on the phonon spectrum starting with the bare phonon frequency and (b) when we already know the adiabatic effects on the phonon spectrum and we want to explore the nonadiabatic effects (e.g., when the starting point is the adiabatic frequency obtained within DFPT [3]).

We start with the usual equations for the electron-ion system [74–76], already separated into Hamiltonians acting on the electron

$$[H_e(\mathbf{r}) + V_{ei}(\mathbf{r},\mathbf{R})]\psi_m(\mathbf{r},\mathbf{R}) = E_m(\mathbf{R})\psi_m(\mathbf{r},\mathbf{R}) \tag{A1}$$

and on the ion wave functions

$$[H_i(\mathbf{R}) + E_n(\mathbf{R})]\phi_n(\mathbf{R}) + \sum_m (\mathcal{A}_{nm} + \mathcal{B}_{nm})\phi_n(\mathbf{R}) = E\phi_n(\mathbf{R}). \tag{A2}$$

In these expressions $H_e(\mathbf{r})$ is the electron Hamiltonian, $H_i(\mathbf{r})$ is the ion Hamiltonian, $V_{ei}(\mathbf{r},\mathbf{R})$ is the interaction that couples the electron charge density to the ions, and

$$\mathcal{A}_{nm} = -\frac{1}{M}\int d\mathbf{r}\psi_m^*(\mathbf{r},\mathbf{R})\nabla_{\mathbf{R}}\psi_m(\mathbf{r},\mathbf{R})\nabla_{\mathbf{R}}, \tag{A3}$$

$$\mathcal{B}_{nm} = -\frac{1}{2M}\int d\mathbf{r}\psi_m^*(\mathbf{r},\mathbf{R})\nabla_{\mathbf{R}}^2\psi_m(\mathbf{r},\mathbf{R}). \tag{A4}$$

By expanding $V_{ei}(\mathbf{r},\mathbf{R})$ for small displacements $\mathbf{Q}_j$ for each ion with index j and then imposing the Bloch theorem and the second quantization we arrive at the operator form for the electron-phonon interaction [74]

$$V_{ep}^{(a)} = \sum_{\mu\mu',\mathbf{kq},\lambda} g_\lambda^{\mu\mu'}(\mathbf{k},\mathbf{q})c_{\mu'\mathbf{k}+\mathbf{q}}^\dagger c_{\mu\mathbf{k}}[b_{\mathbf{q}\lambda} + b_{-\mathbf{q}\lambda}^\dagger], \tag{A5}$$

with the electron-phonon coupling coefficient $g_\lambda^{\mu\mu'}(\mathbf{k},\mathbf{q}) = d_\lambda^{\mu\mu'}(\mathbf{k},\mathbf{q})/\sqrt{2M_\lambda\omega_{\mathbf{q}\lambda}}$, where $d_\lambda^{\mu\mu'}(\mathbf{k},\mathbf{q})$ is the deformation potential defined by Eq. (4). The operators $b_{\mathbf{q}\lambda}$ and $b_{-\mathbf{q}\lambda}^\dagger$ are phonon annihilation and creation operators, respectively. The bare phonon self-energy due to the electron-phonon coupling that corresponds to the interaction $V_{ep}^{(a)}$ is expressed by Eq. (10) where the phonon frequency $\omega_{\mathbf{q}\lambda}$ is actually the bare phonon frequency, $\omega_{\mathbf{q}\lambda} \equiv \omega_{\mathbf{q}\lambda}^0$. Using this self-energy and Eq. (8) we can find the adiabatic

$$\omega_{\mathrm{A}}^2 = \left[\omega_{\mathbf{q}\lambda}^0\right]^2 + 2\omega_{\mathbf{q}\lambda}^0 \mathrm{Re}\pi_\lambda^0(\mathbf{q},0) \tag{A6}$$

and the nonadiabatic phonon frequency

$$\omega_{\mathrm{NA}}^2 = \left[\omega_{\mathbf{q}\lambda}^0\right]^2 + 2\omega_{\mathbf{q}\lambda}^0 \mathrm{Re}\pi_\lambda^0(\mathbf{q},\omega_{\mathrm{NA}}). \tag{A7}$$

A slightly different approach would be to take the interaction operator $\mathcal{A}_{nm}$ acting on the ion wave functions given by Eq. (A3) and express it also in the second quantization form. Note that we are not considering the $\mathcal{B}_{nm}$ operator because it does not affect the phonon spectrum at this level of perturbation expansion [74,75]. To reach the second quantization form we use the Bloch theorem, the off-diagonal Hellmann-Feynman theorem [75,97],

$$\langle\psi_{\mu\mathbf{k}}|\nabla_{\mathbf{R}_j}|\psi_{\mu'\mathbf{k}'}\rangle = -\frac{\langle\psi_{\mu\mathbf{k}}|\frac{\partial V_{ei}}{\partial \mathbf{Q}_{\mathbf{q}\lambda}}|\psi_{\mu'\mathbf{k}'}\rangle}{\varepsilon_{\mu\mathbf{k}} - \varepsilon_{\mu'\mathbf{k}'}}, \tag{A8}$$

and the relation between the ion momentum operator and the phonon creation and annihilation operators, $\nabla_{\mathbf{R}_j} \propto \sqrt{\omega_{\mathbf{q}\lambda}}(b_{-\mathbf{q}\lambda} - b_{\mathbf{q}\lambda}^\dagger)$. Finally, we have

$$V_{ep}^{(b)} \equiv \mathcal{A} = \sum_{\mu\mu',\mathbf{kq},\lambda} \frac{-\omega_{\mathbf{q}\lambda}}{\varepsilon_{\mu\mathbf{k}} - \varepsilon_{\mu'\mathbf{k}+\mathbf{q}}} g_\lambda^{\mu'\mu}(\mathbf{q},\mathbf{k}) \times c_{\mu\mathbf{k}}^\dagger c_{\mu'\mathbf{k}+\mathbf{q}}[b_{-\mathbf{q}\lambda} - b_{\mathbf{q}\lambda}^\dagger], \tag{A9}$$

where $\omega_{\mathbf{q}\lambda}$ is already the adiabatic phonon frequency expressed with Eq. (A6), $\omega_{\mathbf{q}\lambda} \equiv \omega_{\mathrm{A}}$ [75,76]. From the prefactor $\omega_{\mathbf{q}\lambda}/(\varepsilon_{\mu\mathbf{k}} - \varepsilon_{\mu'\mathbf{k}+\mathbf{q}})$ in Eq. (A9) it is clear that the operator $\mathcal{A}$ is a purely nonadiabatic effect (i.e., when $\omega_{\mathbf{q}\lambda} \ll |\varepsilon_{\mu\mathbf{k}} - \varepsilon_{\mu'\mathbf{k}+\mathbf{q}}|$ then $\mathcal{A} \to 0$). Equation (A9) is just the formal notation for the operator $\mathcal{A}$ and we would like to emphasize here that the diagrammatic expansion using this operator as the perturbation Hamiltonian does not exist in the literature to our knowledge [2]. Now we denote the (formal) phonon self-energy associated with $V_{ep}^{(b)}$ as $\widehat{\pi}_\lambda^0(\mathbf{q},\omega)$, and we express the phonon frequency shift due to the nonadiabatic effects in this case as

$$\omega_{\mathrm{NA}}^2 = \omega_{\mathrm{A}}^2 + 2\omega_{\mathrm{A}}\mathrm{Re}\widehat{\pi}_\lambda^0(\mathbf{q},\omega_{\mathrm{NA}}). \tag{A10}$$

Combining Eqs. (A6) and (A7) and comparing the result with Eq. (A10) we get the relation between the real parts of the two phonon self-energies above:

$$\mathrm{Re}\widehat{\pi}_\lambda^0(\mathbf{q},\omega_{\mathrm{NA}}) = \frac{\omega_{\mathbf{q}\lambda}^0}{\omega_{\mathrm{A}}}\left[\mathrm{Re}\pi_\lambda^0(\mathbf{q},\omega_{\mathrm{NA}}) - \mathrm{Re}\pi_\lambda^0(\mathbf{q},0)\right]. \tag{A11}$$

In conclusion, when the starting point is the bare phonon frequency ($\omega_{\mathbf{q}\lambda} \to \omega_{\mathbf{q}\lambda}^0$) it is appropriate to use the real part of the bare phonon self-energy defined with Eq. (10), while when starting with the adiabatic phonon frequency ($\omega_{\mathbf{q}\lambda} \to \omega_{\mathrm{A}}$) the real part of the bare phonon self-energy Eq. (17) should be used.

APPENDIX B: POSSIBLE RTA FORM OF $\widehat{\pi}_\lambda^0$

Since the usual starting point of the contemporary nonadiabatic calculations is the phonon self-energy with adiabatic phonon frequency and finite numerical broadening parameter $\eta > 0$, it would be useful to have the RTA form of $\widehat{\pi}_\lambda^0$ obtained with Eq. (17) where its imaginary part is equal to the imaginary part of Eq. (10) in the RTA, i.e., $\mathrm{Im}\widehat{\pi}_\lambda^0(\omega) = \mathrm{Im}\pi_\lambda^0(\omega)$. Since the direct diagrammatic perturbation expansion of $\widehat{\pi}_\lambda^0$ has not been developed to our knowledge, we take a different

approach here. First we account for all the relevant electron scattering processes (at least formally) in the phonon self-energy $\Pi_\lambda(\omega)$ and then we subtract the adiabatic term in the clean noninteracting limit $\pi^0_\lambda(0)$. In that way, we avoid the direct perturbation expansion of $\widehat{\pi}^0_\lambda$ by constructing $\widehat{\Pi}_\lambda$ *a posteriori*. In Matsubara notation this reads

$$\begin{aligned}\widehat{\Pi}_\lambda(\mathbf{q},i\nu_n) &= \Pi_\lambda(\mathbf{q},i\nu_n) - \pi^0_\lambda(\mathbf{q},0)\\ &= \sum_{\mu\mu'\mathbf{k}\sigma}\frac{1}{\beta}\sum_{i\omega_n}\left[g^{\mu\mu'}_\lambda(\mathbf{k},\mathbf{q})\right]^*\widetilde{g}^{\mu\mu'}_\lambda(\mathbf{k},\mathbf{q})\\ &\quad\times\frac{G_\mu(\mathbf{k})-G_{\mu'}(\mathbf{k}+\mathbf{q})}{i\nu_n+\varepsilon_{\mu\mathbf{k}}-\varepsilon_{\mu'\mathbf{k}+\mathbf{q}}+\Delta\Sigma_{\mu\mu'}(\mathbf{k},\mathbf{q})}\\ &\quad-\sum_{\mu\mu'\mathbf{k}\sigma}\frac{1}{\beta}\sum_{i\omega_n}\left|g^{\mu\mu'}_\lambda(\mathbf{k},\mathbf{q})\right|^2\frac{G^0_\mu(\mathbf{k})-G^0_{\mu'}(\mathbf{k}+\mathbf{q})}{\varepsilon_{\mu\mathbf{k}}-\varepsilon_{\mu'\mathbf{k}+\mathbf{q}}},\end{aligned} \tag{B1}$$

where dependence on $i\omega_n$ and $i\nu_n$ is assumed in $\widetilde{g}_\lambda$, G, and $\Delta\Sigma$. In the simplest RTA form (as described in Sec. II B), Eq. (B1) can be expressed as

$$\begin{aligned}\widehat{\pi}^{0,\mathrm{RTA}}_\lambda(\mathbf{q},\omega) &= \sum_{\mu\mu'\mathbf{k}\sigma}\left|g^{\mu\mu'}_\lambda(\mathbf{k},\mathbf{q})\right|^2\\ &\quad\times\frac{f_{\mu\mathbf{k}}-f_{\mu'\mathbf{k}+\mathbf{q}}}{\varepsilon_{\mu\mathbf{k}}-\varepsilon_{\mu'\mathbf{k}+\mathbf{q}}}\,\frac{-(\omega+i\Gamma)}{\omega+\varepsilon_{\mu\mathbf{k}}-\varepsilon_{\mu'\mathbf{k}+\mathbf{q}}+i\Gamma},\end{aligned} \tag{B2}$$

where the corresponding imaginary and real parts are

$$\begin{aligned}\mathrm{Im}\widehat{\pi}^{0,\mathrm{RTA}}_\lambda(\mathbf{q},\omega) &= \sum_{\mu\mu'\mathbf{k}\sigma}\left|g^{\mu\mu'}_\lambda(\mathbf{k},\mathbf{q})\right|^2(f_{\mu\mathbf{k}}-f_{\mu'\mathbf{k}+\mathbf{q}})\\ &\quad\times\frac{-\Gamma}{(\omega+\varepsilon_{\mu\mathbf{k}}-\varepsilon_{\mu'\mathbf{k}+\mathbf{q}})^2+\Gamma^2}\end{aligned} \tag{B3}$$

and

$$\begin{aligned}\mathrm{Re}\widehat{\pi}^{0,\mathrm{RTA}}_\lambda(\mathbf{q},\omega) &= -\sum_{\mu\mu'\mathbf{k}\sigma}\left|g^{\mu\mu'}_\lambda(\mathbf{k},\mathbf{q})\right|^2\frac{f_{\mu\mathbf{k}}-f_{\mu'\mathbf{k}+\mathbf{q}}}{\varepsilon_{\mu\mathbf{k}}-\varepsilon_{\mu'\mathbf{k}+\mathbf{q}}}\\ &\quad\times\frac{\omega(\omega+\varepsilon_{\mu\mathbf{k}}-\varepsilon_{\mu'\mathbf{k}+\mathbf{q}})-\Gamma^2}{(\omega+\varepsilon_{\mu\mathbf{k}}-\varepsilon_{\mu'\mathbf{k}+\mathbf{q}})^2+\Gamma^2}.\end{aligned} \tag{B4}$$

We can see that the imaginary part of Eq. (B2) gives the same result as the RTA form of $\mathrm{Im}\pi^0_\lambda(\omega)$, while the real part gives directly the nonadiabatic correction to the adiabatic phonon frequency. The superscript RTA is used here to distinguish Eq. (B2) from Eq. (23).

APPENDIX C: EQUATION OF MOTION FOR THE TWO-PARTICLE PROPAGATOR

The analytically continued equation for the exact phonon self-energy [Eq. (3)] can be expressed explicitly with the two-particle propagator $\mathcal{G}_{\mu\mu'}$ in the following way:

$$\begin{aligned}\Pi_\lambda(\mathbf{q},\omega) &= \sum_{\mu\mu'\mathbf{k}\sigma}\left[g^{\mu\mu'}_\lambda(\mathbf{k},\mathbf{q})\right]^* g^{\mu\mu'}_\lambda(\mathbf{k}_1,\mathbf{q})\\ &\quad\times\mathcal{G}_{\mu\mu'}(\mathbf{k},\mathbf{k}_+,\mathbf{k}_1,\mathbf{k}_{1+},\omega),\end{aligned} \tag{C1}$$

where $\mathbf{k}_+$ and $\mathbf{k}_{1+}$ stand for $\mathbf{k}+\mathbf{q}$ and $\mathbf{k}_1+\mathbf{q}$, respectively. Here we gather all the relevant vertex correction contributions into $\mathcal{G}_{\mu\mu'}$, while in Eq. (3) they are in one of the vertex functions. Within the usual equation of motion approach for the propagators, it is customary to start with the time-dependent form of $\mathcal{G}_{\mu\mu'}$

$$\begin{aligned}&\mathcal{G}_{\mu\mu'}(\mathbf{k},\mathbf{k}_+,\mathbf{k}_1,\mathbf{k}_{1+},t)\\ &\quad=-i\theta(t)\left\langle\left[A^{\mu\mu'}_{\mathbf{kq}\sigma}(t),B^{\mu\mu'}_{\mathbf{k}_1\mathbf{q}\sigma}(0)\right]\right\rangle\\ &\quad=\int_{-\infty}^{\infty}\frac{d\omega}{2\pi}e^{i\omega t-\eta t}\mathcal{G}_{\mu\mu'}(\mathbf{k},\mathbf{k}_+,\mathbf{k}_1,\mathbf{k}_{1+},\omega),\end{aligned} \tag{C2}$$

where the Heisenberg operators are defined as

$$A^{\mu\mu'}_{\mathbf{kq}\sigma}(t)=c^\dagger_{\mu\mathbf{k}\sigma}(t)c_{\mu'\mathbf{k}+\mathbf{q}\sigma}(t) \tag{C3}$$

and

$$B^{\mu\mu'}_{\mathbf{k}_1\mathbf{q}\sigma}(0)=c^\dagger_{\mu'\mathbf{k}_1\sigma}(0)c_{\mu\mathbf{k}_1+\mathbf{q}\sigma}(0), \tag{C4}$$

with $c^\dagger_{\mu\mathbf{k}\sigma}(t)$ and $c_{\mu\mathbf{k}\sigma}(t)$ being the electron creation and annihilation operators, respectively. In our present analysis for an electron-phonon system with impurities, the Hamiltonian can be written as

$$H=H_e+H_p+V_{ep}+V_{\mathrm{imp}}, \tag{C5}$$

where H_e and H_p are the usual adiabatic electron and phonon Hamiltonians, V_{ep} is the electron-phonon coupling given by Eq. (A5), and

$$V_{\mathrm{imp}}=\sum_{\mu\mathbf{k}\mathbf{k}_1\sigma}V(\mathbf{k}-\mathbf{k}_1)c^\dagger_{\mu\mathbf{k}\sigma}c_{\mu\mathbf{k}_1\sigma} \tag{C6}$$

represents the quasielastic single-electron scattering processes on the impurities, which are restricted to the intraband contributions only. We can write now the equation of motion as [49,98]

$$\begin{aligned}&i\frac{d}{dt}\mathcal{G}_{\mu\mu'}(\mathbf{k},\mathbf{k}_+,\mathbf{k}_1,\mathbf{k}_{1+},t)\\ &\quad=\delta(t)\delta_{\mathbf{k},\mathbf{k}_1}(f_{\mu\mathbf{k}}-f_{\mu'\mathbf{k}+\mathbf{q}})\\ &\qquad-(\varepsilon_{\mu\mathbf{k}}-\varepsilon_{\mu'\mathbf{k}+\mathbf{q}})\mathcal{G}_{\mu\mu'}(\mathbf{k},\mathbf{k}_+,\mathbf{k}_1,\mathbf{k}_{1+},t)\\ &\qquad-i\theta(t)\left\langle\left[\left[A^{\mu\mu'}_{\mathbf{kq}\sigma}(t),H'\right],B^{\mu\mu'}_{\mathbf{k}_1\mathbf{q}\sigma}(0)\right]\right\rangle,\end{aligned} \tag{C7}$$

where $H'=V_{ep}+V_{\mathrm{imp}}$. In the present work we are mostly interested in the long-wavelength part of the phonon self-energy; thus $\mathbf{q}=0$ should be used throughout in Eq. (C7). Furthermore, we restrict our consideration to the intraband transitions ($\mu=\mu'$) for which the first and second terms are zero and we neglect as well the V_{ep} part in the last term (i.e., we disregard the higher-order electron-phonon processes). After performing the Fourier transform of Eq. (C7) we get

$$\begin{aligned}&\omega\mathcal{G}_{\mu\mu}(\mathbf{k},\mathbf{k},\mathbf{k}_1,\mathbf{k}_1,\omega)\\ &\quad=-i\int_{-\infty}^{\infty}dt e^{-i\omega t}\theta(t)\left\langle\left[\left[A^{\mu\mu}_{\mathbf{k}\sigma}(t),V_{\mathrm{imp}}\right],B^{\mu\mu}_{\mathbf{k}_1\sigma}(0)\right]\right\rangle\\ &\quad\equiv\left\langle\left\langle\left[A^{\mu\mu}_{\mathbf{k}\sigma},V_{\mathrm{imp}}\right];B^{\mu\mu}_{\mathbf{k}_1\sigma}\right\rangle\right\rangle_\omega.\end{aligned} \tag{C8}$$

The next step is to use the equation of motion Eq. (C7) but now for the propagator at the right-hand side of Eq. (C8). By

doing this we can express Eq. (C8) as

$$\omega\mathcal{G}_{\mu\mu}(\mathbf{k},\mathbf{k},\mathbf{k}_1,\mathbf{k}_1,\omega) = \frac{1}{\omega}\langle\langle\left[A^{\mu\mu}_{\mathbf{k}\sigma}, V_{\rm imp}\right]; B^{\mu\mu}_{\mathbf{k}_1\sigma}\rangle\rangle - \frac{1}{\omega}\langle\langle\left[A^{\mu\mu}_{\mathbf{k}\sigma}, V_{\rm imp}\right]; \left[B^{\mu\mu}_{\mathbf{k}_1\sigma}, V_{\rm imp}\right]\rangle\rangle_{\omega}, \tag{C9}$$

where the second term on the right-hand side is the propagator part of the force-force correlation function [49,55,61],

$$\Phi_{\mu\mu}(\mathbf{k},\mathbf{k},\mathbf{k}_1,\mathbf{k}_1,\omega) = \langle\langle\left[A^{\mu\mu}_{\mathbf{k}\sigma}, V_{\rm imp}\right]; \left[B^{\mu\mu}_{\mathbf{k}_1\sigma}, V_{\rm imp}\right]\rangle\rangle_{\omega}. \tag{C10}$$

By taking the formal limit $\omega = 0$ we can express the two-particle propagator solely through the force-force correlation function

$$\mathcal{G}_{\mu\mu}(\mathbf{k},\mathbf{k},\mathbf{k}_1,\mathbf{k}_1,\omega) = -\frac{1}{\omega^2}[\Phi_{\mu\mu}(\mathbf{k},\mathbf{k},\mathbf{k}_1,\mathbf{k}_1,\omega) - \Phi_{\mu\mu}(\mathbf{k},\mathbf{k},\mathbf{k}_1,\mathbf{k}_1,0)]. \tag{C11}$$

Finally, if we include Eq. (C11) into Eq. (C1) we get the force-force correlation function approach for obtaining the $\mathbf{q} \approx 0$ intraband phonon self-energy [Eq. (37)].

APPENDIX D: JDOS AND LORENTZIANS

We define the complex joint density of states (JDOS) for the $\mathbf{q} \approx 0$ interband parts of functions Eq. (10) and Eq. (17) using the function

$$\Lambda^{\rm inter}_{\varphi}(\mathbf{q}\approx 0,\omega) = \sum_{\mu\neq\mu',\mathbf{k}} \varphi^{-1}\frac{f_{\mu\mathbf{k}} - f_{\mu'\mathbf{k}}}{\omega + \varepsilon_{\mu\mathbf{k}} - \varepsilon_{\mu'\mathbf{k}} + i\Gamma_{\rm inter}}, \tag{D1}$$

which for $\varphi = \omega$ is the JDOS related to Eq. (10), and for $\varphi = \varepsilon_{\mu'\mathbf{k}} - \varepsilon_{\mu\mathbf{k}} \equiv \Delta\varepsilon$ is the JDOS corresponding to Eq. (17). Note that Eqs. (10) and (D1) have a similar functional dependence on ω only if we consider that $\omega_{0\lambda} \to \omega$ in the matrix elements $g^{\mu\mu'}_{\lambda}$ of Eq. (10). The imaginary and real parts of these JDOS functions for different damping energies $\Gamma_{\rm inter}$ and number of Cu layers can qualitatively predict the behavior of the phonon linewidths and frequency shifts as a function of these parameters. It can also be seen what the difference between the imaginary part of the self-energy with $\varphi = \omega$ and with $\varphi = \varepsilon_{\mu'\mathbf{k}} - \varepsilon_{\mu\mathbf{k}}$ is. In Figs. 11(a) and 11(c) we see how the imaginary part of the JDOS obtained for the CO stretch mode increases when increasing the number of Cu layers (compare with Fig. 9). The effect of different damping energies $\Gamma_{\rm inter}$ on the imaginary part of the JDOS is shown in Figs. 11(b) and 11(d). The overall difference between the JDOS obtained with $\varphi = \omega$ (left panels in Fig. 11) and with $\varphi = \varepsilon_{\mu'\mathbf{k}} - \varepsilon_{\mu\mathbf{k}}$ (right panels in Fig. 11) is that the latter gives smaller values than the former for the same damping energies $\Gamma_{\rm inter}$, which is in agreement with the results presented in Fig 6. Additionally, we show the results for the real part of the JDOS for different number of Cu layers and temperatures in Figs. 12(a) and 12(b), respectively. The result for different numbers of Cu layers is in agreement with the result obtained in Fig. 10, where the real part of the interband phonon self-energy does not change drastically with the number of layers.

The differences and similarities between the methods used in Fig. 6 can be further clarified by looking at the corresponding Lorentzians:

(1) Lorentzian corresponding to Eq. (47)

$$\mathcal{L}^{(1)}_{\Gamma_{\rm inter}}(\Delta\varepsilon) = \frac{1}{|\Delta\varepsilon|}\frac{\Gamma_{\rm inter}}{\Delta\varepsilon^2 + \Gamma^2_{\rm inter}}, \tag{D2}$$

(2) Lorentzian corresponding to Eq. (48)

$$\mathcal{L}^{(2)}_{\Gamma_{\rm inter}}(\Delta\varepsilon) = \frac{2\Gamma_{\rm inter}|\Delta\varepsilon|}{\left[\Delta\varepsilon^2 + \Gamma^2_{\rm inter}\right]^2}, \tag{D3}$$

(3) Lorentzian corresponding to the imaginary part of Eq. (17)

$$\mathcal{L}^{(3)}_{\Gamma_{\rm inter}}(\Delta\varepsilon,\omega_{0\lambda}) = \frac{1}{|\Delta\varepsilon|}\frac{\Gamma_{\rm inter}}{(\omega_{0\lambda} - |\Delta\varepsilon|)^2 + \Gamma^2_{\rm inter}}, \tag{D4}$$

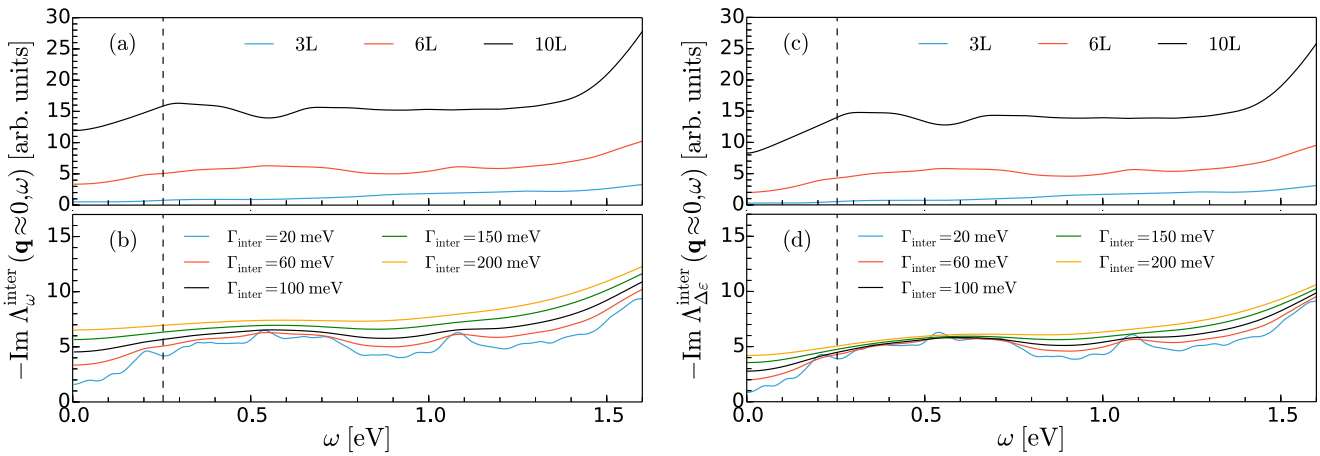

FIG. 11. Imaginary part of the JDOS Eq. (D1) with $\varphi = \omega$ as a function of ω for (a) different numbers of Cu layers with $\Gamma_{\rm inter} = 60$ meV and (b) different damping energies $\Gamma_{\rm inter}$ with six Cu layers. Panels (c) and (d) show the same quantities as (a) and (b), respectively, but with $\varphi = \Delta\varepsilon$. The dashed vertical lines represent the energy of the CO stretch mode.

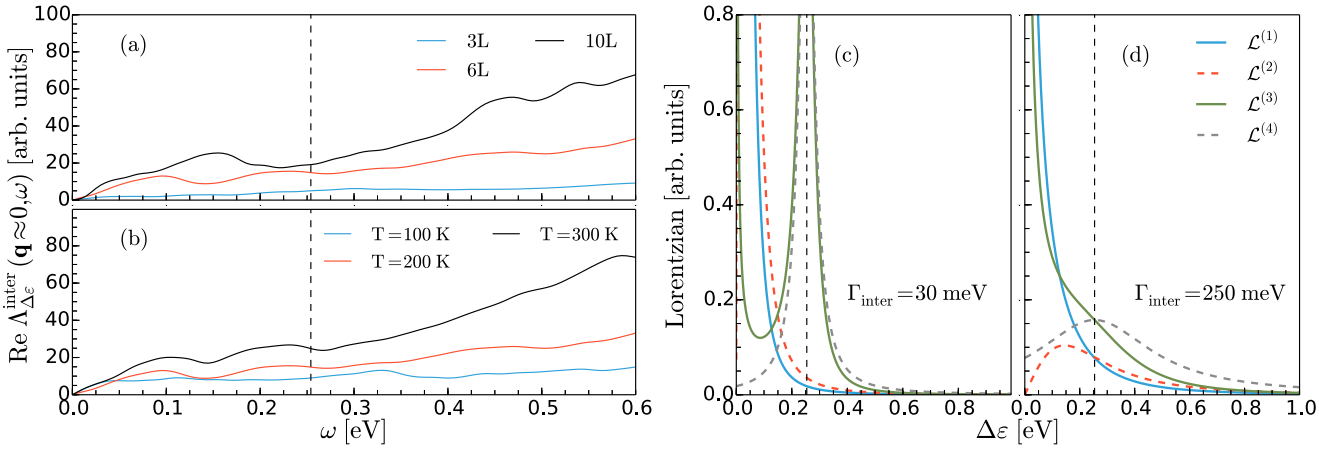

FIG. 12. Real part of the JDOS Eq. (D1) as a function of ω for (a) different number of Cu layers with $T = 200$ K and (b) different temperatures with six Cu layers, where $\varphi = \Delta\varepsilon$. Different types of Lorentzians as a function of excitation energy $\Delta\varepsilon$ for (c) $\Gamma_{\text{inter}} = 30$ meV and (d) $\Gamma_{\text{inter}} = 250$ meV. The dashed vertical lines represent the energy of the CO stretch mode.

(4) Lorentzian corresponding to the imaginary part of Eq. (10)

$$\mathcal{L}^{(4)}_{\Gamma_{\text{inter}}}(\Delta\varepsilon,\omega_{0\lambda}) = \frac{1}{\omega_{0\lambda}}\frac{\Gamma_{\text{inter}}}{(\omega_{0\lambda}-|\Delta\varepsilon|)^2+\Gamma^2_{\text{inter}}}. \tag{D5}$$

Here we consider the energy difference $\Delta\varepsilon$ and damping energy Γ_{inter} as free parameters, while the phonon frequency $\omega_{0\lambda}$ is the one for the CO stretch mode. It can be seen that $\mathcal{L}^{(1)}_{\Gamma_{\text{inter}}} \approx \mathcal{L}^{(2)}_{\Gamma_{\text{inter}}}$ and $\mathcal{L}^{(3)}_{\Gamma_{\text{inter}}} \approx \mathcal{L}^{(4)}_{\Gamma_{\text{inter}}}$ for small values of Γ_{inter} [Fig. 12(c)], while $\mathcal{L}^{(1)}_{\Gamma_{\text{inter}}} \approx \mathcal{L}^{(3)}_{\Gamma_{\text{inter}}}$ and $\mathcal{L}^{(2)}_{\Gamma_{\text{inter}}} \approx \mathcal{L}^{(4)}_{\Gamma_{\text{inter}}}$ for large values of Γ_{inter} [Fig. 12(d)]. The similar form of the Lorentzians $\mathcal{L}^{(2)}_{\Gamma_{\text{inter}}}$ and $\mathcal{L}^{(4)}_{\Gamma_{\text{inter}}}$ for large Γ_{inter} is accidental and for a different value of $\omega_{0\lambda}$ they would be different. For values $\Gamma_{\text{inter}} < 150$ meV the difference between $\mathcal{L}^{(1,2)}_{\Gamma_{\text{inter}}}$ (quasistatic limits) and $\mathcal{L}^{(3,4)}_{\Gamma_{\text{inter}}}$ is very pronounced (in the same way there is a difference between the different $\gamma^{\text{inter}}_{0\lambda}$ curves for small Γ_{inter} in Fig. 6).

[1] M. Born and R. Oppenheimer, Ann. Phys. **389**, 457 (1927).
[2] E. G. Maksimov and A. E. Karakozov, Phys. Usp. **51**, 535 (2008).
[3] S. Baroni, S. de Gironcoli, A. Dal Corso, and P. Giannozzi, Rev. Mod. Phys. **73**, 515 (2001).
[4] S. Engelsberg and J. R. Schrieffer, Phys. Rev. **131**, 993 (1963).
[5] I. P. Ipatova and A. V. Subashiev, Zh. Eksp. Teor. Fiz. **66**, 722 (1974) [JETP **39**, 349 (1974)].
[6] F. Marsiglio, R. Akis, and J. P. Carbotte, Phys. Rev. B **45**, 9865 (1992).
[7] E. Maksimov and S. Shulga, Solid State Commun. **97**, 553 (1996).
[8] Y. S. Ponosov, G. A. Bolotin, C. Thomsen, and M. Cardona, Phys. Status Solidi B **208**, 257 (1998).
[9] G. A. Bolotin, Y. I. Kuz'min, Y. V. Knyazev, Y. S. Ponosov, and C. Thomsen, Phys. Solid State **43**, 1801 (2001).
[10] A. M. Saitta, M. Lazzeri, M. Calandra, and F. Mauri, Phys. Rev. Lett. **100**, 226401 (2008).
[11] M. Lazzeri and F. Mauri, Phys. Rev. Lett. **97**, 266407 (2006).
[12] T. Ando, J. Phys. Soc. Jpn. **75**, 124701 (2006).
[13] C. A. Howard, M. P. M. Dean, and F. Withers, Phys. Rev. B **84**, 241404 (2011).
[14] G. Froehlicher and S. Berciaud, Phys. Rev. B **91**, 205413 (2015).
[15] H. Ueba, Prog. Surf. Sci. **55**, 115 (1997).
[16] H. Nienhaus, H. Bergh, B. Gergen, A. Majumdar, W. Weinberg, and E. McFarland, Surf. Sci. **445**, 335 (2000).
[17] B. Gergen, H. Nienhaus, W. H. Weinberg, and E. W. McFarland, Science **294**, 2521 (2001).
[18] H. Nienhaus, Surf. Sci. Rep. **45**, 1 (2002).
[19] Y. Huang, C. T. Rettner, D. J. Auerbach, and A. M. Wodtke, Science **290**, 111 (2000).
[20] J. D. White, J. Chen, D. Matsiev, D. J. Auerbach, and A. M. Wodtke, Nature (London) **433**, 503 (2005).
[21] D. Novko, M. Blanco-Rey, J. I. Juaristi, and M. Alducin, Phys. Rev. B **92**, 201411 (2015).
[22] D. Novko, M. Blanco-Rey, J. Juaristi, and M. Alducin, Nucl. Instrum. Methods Phys. Res., Sect. B **382**, 26 (2016).
[23] D. Novko, M. Blanco-Rey, M. Alducin, and J. I. Juaristi, Phys. Rev. B **93**, 245435 (2016).
[24] M. Blanco-Rey, J. I. Juaristi, R. Díez Muiño, H. F. Busnengo, G. J. Kroes, and M. Alducin, Phys. Rev. Lett. **112**, 103203 (2014).
[25] J. I. Juaristi, M. Alducin, R. Díez Muiño, H. F. Busnengo, and A. Salin, Phys. Rev. Lett. **100**, 116102 (2008).
[26] S. P. Rittmeyer, J. Meyer, J. I. Juaristi, and K. Reuter, Phys. Rev. Lett. **115**, 046102 (2015).
[27] L. Martin-Gondre, M. Alducin, G. A. Bocan, R. Díez Muiño, and J. I. Juaristi, Phys. Rev. Lett. **108**, 096101 (2012).
[28] P. Saalfrank, J. I. Juaristi, M. Alducin, M. Blanco-Rey, and R. Díez Muiño, J. Chem. Phys. **141**, 234702 (2014).

[29] O. Galparsoro, R. Pétuya, J. I. Juaristi, C. Crespos, M. Alducin, and P. Larregaray, J. Phys. Chem. C **119**, 15434 (2015).

[30] I. Lončarić, M. Alducin, P. Saalfrank, and J. I. Juaristi, Phys. Rev. B **93**, 014301 (2016).

[31] B. Persson and M. Persson, Solid State Commun. **36**, 175 (1980).

[32] B. Hellsing and M. Persson, Phys. Scr. **29**, 360 (1984).

[33] T. T. Rantala and A. Rosén, Phys. Rev. B **34**, 837 (1986).

[34] N. Lorente and M. Persson, Faraday Discuss. **117**, 277 (2000).

[35] J. Trail, M. Graham, and D. Bird, Comput. Phys. Commun. **137**, 163 (2001).

[36] V. Krishna and J. C. Tully, J. Chem. Phys. **125**, 054706 (2006).

[37] M. Forsblom and M. Persson, J. Chem. Phys. **127**, 154303 (2007).

[38] J. C. Tremblay, S. Monturet, and P. Saalfrank, Phys. Rev. B **81**, 125408 (2010).

[39] S. Monturet and P. Saalfrank, Phys. Rev. B **82**, 075404 (2010).

[40] J. C. Tremblay, J. Chem. Phys. **138**, 244106 (2013).

[41] M. Askerka, R. J. Maurer, V. S. Batista, and J. C. Tully, Phys. Rev. Lett. **116**, 217601 (2016).

[42] R. J. Maurer, M. Askerka, V. S. Batista, and J. C. Tully, Phys. Rev. B **94**, 115432 (2016).

[43] M. Blanco-Rey, M. Alducin, J. I. Juaristi, and P. L. de Andres, Phys. Rev. Lett. **108**, 115902 (2012).

[44] P. N. Keating, Phys. Rev. **175**, 1171 (1968).

[45] Ž. Crljen and D. C. Langreth, Phys. Rev. B **35**, 4224 (1987).

[46] V. L. Aksenov and V. V. Kabanov, Phys. Rev. B **57**, 608 (1998).

[47] E. Cappelluti, Phys. Rev. B **73**, 140505 (2006).

[48] M. Calandra and F. Mauri, Phys. Rev. B **71**, 064501 (2005).

[49] W. Götze and P. Wölfle, Phys. Rev. B **6**, 1226 (1972).

[50] J. Ruvalds and A. Virosztek, Phys. Rev. B **43**, 5498 (1991).

[51] P. B. Allen, Phys. Rev. B **3**, 305 (1971).

[52] P. B. Allen, Phys. Rev. B **92**, 054305 (2015).

[53] I. Kupčić, Phys. Rev. B **91**, 205428 (2015).

[54] D. Novko, M. Šunjić, and V. Despoja, Phys. Rev. B **93**, 125413 (2016).

[55] G. D. Mahan, *Many-Particle Physics*, 3rd ed. (Plenum, New York, 2000).

[56] A. Zawadowski and M. Cardona, Phys. Rev. B **42**, 10732 (1990).

[57] V. N. Kostur, Z. Phys. B **89**, 149 (1992).

[58] A. Virosztek and J. Ruvalds, Phys. Rev. B **45**, 347 (1992).

[59] L. A. Falkovsky, Zh. Eksp. Teor. Fiz. **103**, 666 (1993) [JETP **76**, 331 (1993)].

[60] I. Kupčić and S. Barišić, Phys. Rev. B **75**, 094508 (2007).

[61] I. Kupčić, Phys. Rev. B **79**, 235104 (2009).

[62] B. Chakraborty and P. B. Allen, Phys. Rev. B **18**, 5225 (1978).

[63] E. Riccardi, M.-A. Méasson, M. Cazayous, A. Sacuto, and Y. Gallais, Phys. Rev. Lett. **116**, 066805 (2016).

[64] R. Ryberg, Phys. Rev. B **32**, 2671 (1985).

[65] T. A. Germer, J. C. Stephenson, E. J. Heilweil, and R. R. Cavanagh, J. Chem. Phys. **101**, 1704 (1994).

[66] B. N. J. Persson, J. Phys. C **17**, 4741 (1984).

[67] M. Morin, N. J. Levinos, and A. L. Harris, J. Chem. Phys. **96**, 3950 (1992).

[68] Although it was not studied to a great extent, the problem of finite broadening of electronic states has been addressed earlier in the context of nonadiabatic effects in gas-surface dynamics [33,99] .

[69] A. A. Abrikosov, L. P. Gorkov, and I. E. Dzyaloshinski, *Methods of Quantum Field Theory in Statistical Physics* (Dover, New York, 1975).

[70] F. Giustino, arXiv:1603.06965.

[71] V. Despoja, D. Novko, K. Dekanić, M. Šunjić, and L. Marušić, Phys. Rev. B **87**, 075447 (2013).

[72] D. Novko, V. Despoja, and M. Šunjić, Phys. Rev. B **91**, 195407 (2015).

[73] D. Pines and P. Noziéres, *The Theory of Quantum Liquids I* (Addison-Wesley, New York, 1989).

[74] G. Grimvall, *The Electron-Phonon Interaction in Metals* (North-Holland, Amsterdam, 1981).

[75] E. G. Brovman and Yu. Kagan, Zh. Eksp. Teor. Fiz. **52**, 557 (1967) [JETP **25**, 365 (1967)].

[76] B. T. Geilikman, J. Low Temp. Phys. **4**, 189 (1971).

[77] T. Ando, J. Phys. Soc. Jpn. **76**, 024712 (2007).

[78] J. Dietel and H. Kleinert, Phys. Rev. B **82**, 195437 (2010).

[79] M. Calandra, G. Profeta, and F. Mauri, Phys. Rev. B **82**, 165111 (2010).

[80] P. Zhang, S. G. Louie, and M. L. Cohen, Phys. Rev. Lett. **94**, 225502 (2005).

[81] S. Huotari, J. A. Soininen, T. Pylkkänen, K. Hämäläinen, A. Issolah, A. Titov, J. McMinis, J. Kim, K. Esler, D. M. Ceperley, M. Holzmann, and V. Olevano, Phys. Rev. Lett. **105**, 086403 (2010).

[82] T. Holstein, Ann. Phys. **29**, 410 (1964).

[83] Y. S. Ponosov and S. V. Streltsov, Phys. Rev. B **86**, 045138 (2012).

[84] H. Morawitz, Phys. Rev. Lett. **58**, 2778 (1987).

[85] E. Cappelluti and L. Pietronero, Phys. C (Amsterdam, Neth.) **460-462**, Part 1, 70 (2007).

[86] P. B. Allen, Phys. Rev. B **6**, 2577 (1972).

[87] This result is in close analogy to the behavior of the direct current conductivity formula $\sigma(\omega = 0)$, that fulfills $\mathrm{Re}\sigma(\omega = 0) \to +\infty$ in the $\eta \to 0^+$ limit. In both cases, the divergence comes from the fact that both $\mathrm{Re}\sigma(\omega = 0)$ and $\mathrm{Im}\pi^0_\lambda(\omega_{0\lambda} = 0)$ are proportional to η^{-1} [55]. Physically, this would mean that the system has an ideal direct current conductivity in the clean noninteracting limit and that any external perturbation could excite an infinite number of electron-hole pairs. Thus, in our case an external perturbation such as $\omega_{0\lambda} \approx 0$ phonons would have an infinite damping, which is clearly nonphysical.

[88] P. Giannozzi, S. Baroni, N. Bonini, M. Calandra, R. Car, C. Cavazzoni, D. Ceresoli, G. L. Chiarotti, M. Cococcioni, I. Dabo *et al.*, J. Phys.: Condens. Matter **21**, 395502 (2009).

[89] Y. Zhang and W. Yang, Phys. Rev. Lett. **80**, 890 (1998).

[90] We have checked that different exchange and correlation functionals do not change significantly the value of phonon linewidth. We used the following functionals to test this: revPBE, PBE [100], LDA [101], and WC [102].

[91] H. J. Monkhorst and J. D. Pack, Phys. Rev. B **13**, 5188 (1976).

[92] S. Andersson and J. B. Pendry, Phys. Rev. Lett. **43**, 363 (1979).

[93] G. Teobaldi, M. Peñalba, A. Arnau, N. Lorente, and W. A. Hofer, Phys. Rev. B **76**, 235407 (2007).

[94] I. Kupčić, Phys. Rev. B **90**, 205426 (2014).

[95] N. W. Ashcroft and N. D. Mermin, *Solid State Physics*, 1st ed. (Brooks Cole, 1976).

[96] The adiabatic frequency for the CO stretch mode on Cu(100) approximated with six layers obtained with the PBE functional is $\omega^{\mathrm{PBE}}_{0\lambda} = 61.66$ THz, while with the nonlocal vdW-DF

corrected value [103,104] it is $\omega_{0\lambda}^{\mathrm{vdW-DF}} = 60.56\,\mathrm{THz}$. These results are respectively slightly higher and lower than the revPBE result, $\omega_{0\lambda}^{\mathrm{revPBE}} = 61.41\,\mathrm{THz}$.

[97] M. Born and V. Fock, Z. Phys. **51**, 165 (1928).

[98] R. Kubo, M. Toda, and N. Hashitsume, *Statistical Physics II: Nonequilibrium Statistical Mechanics* (Springer-Verlag, Berlin, 1991).

[99] B. Lindgren and D. E. Ellis, Phys. Rev. B **26**, 636 (1982).

[100] J. P. Perdew, K. Burke, and M. Ernzerhof, Phys. Rev. Lett. **77**, 3865 (1996).

[101] J. P. Perdew and A. Zunger, Phys. Rev. B **23**, 5048 (1981).

[102] Z. Wu and R. E. Cohen, Phys. Rev. B **73**, 235116 (2006).

[103] M. Dion, H. Rydberg, E. Schröder, D. C. Langreth, and B. I. Lundqvist, Phys. Rev. Lett. **92**, 246401 (2004).

[104] T. Thonhauser, V. R. Cooper, S. Li, A. Puzder, P. Hyldgaard, and D. C. Langreth, Phys. Rev. B **76**, 125112 (2007).